Chapter 6
Estimation of the impacts of climate change on carbon dynamics in terrestrial ecosystems

6.1. Introduction

The CO_2 emission from human activities to the atmosphere will critically affect the terrestrial ecosystems through the greenhouse effect on climate system and the CO_2 fertilization effect on plant productivity. These impacts on terrestrial ecosystems may range from the molecular scale (Van Oosten et al., 1994) to the biosphere scale (Vitousek, 1994). However, the response of terrestrial ecosystems may be so large that the feedback effect would in turn alter the atmospheric CO_2 concentration and climate condition (Martin, 1993; Melillo et al., 1996; Woodward et al., 1998). For example, if the plant photosynthesis is enhanced by a few percent globally, almost all of the industry CO_2 emission (5.5 Pg C yr^{-1}; IPCC, 1996) may be sequestered into the biosphere. Quantifying the atmosphere-biosphere interaction is difficult, especially at the global scale, although several studies have summarized the plant response to elevated CO_2 concentration (Poorter, 1993; Idso and Idso, 1994; Wullschleger et al., 1995; Curtis and Wang, 1998).

Using a simulation model of terrestrial carbon cycle is one of the promising procedures to estimate and analyze the atmosphere-biosphere interaction (Esser, 1987; Raich et al., 1991; Potter et al., 1993; Running and Hunt, 1993; Foley, 1994a; Ludeke et al., 1994; Warnant et al., 1994; Den Elzen et al., 1997; Cao and Woodward, 1998b; Xiao et al., 1998). These models have been used to estimate the spatial and temporal distribution of primary productivity and carbon storage, and to simulate the response to global warming induced by increased CO_2 (Kohlmaier et al., 1995; Melillo, 1996; Cao and Woodward, 1998a). Moreover, some models have been used to seek the missing carbon sink (Dai and Fung, 1993; King et al., 1995), to compare the interannual change in carbon budget (Kaduk and Heimann, 1994; Kindermann et al., 1996; Gérard et al., 1999), and to reproduce the past terrestrial ecosystems (Foley, 1994b; Esser and Lautenschlager, 1994). Most models consider the regulation of productivity by radiation, temperature, water availability, and atmospheric CO_2 concentration,

in various ways (Pan et al., 1998; Churkina et al., 1999); some models, in addition, include the regulation by nitrogen availability (McGuire et al., 1997).

In this Chapter, a series of simulations are performed to estimate the changes in productivity and carbon storage of terrestrial ecosystems. Sim-CYCLE may enable us to estimate the spatio-temporal distribution of atmosphere-biosphere CO_2 exchange at the global scale. After the Industrial Revolution, atmospheric CO_2 concentration has increased from 275 to 360 ppmv (Neftel et al., 1985; Keeling et al., 1995), and this may cause a significant degree of global warming (Jones et al., 1999). The extrapolation of environmental condition to the future remains uncertainties. However, several prescribed scenarios of the atmospheric CO_2 concentration are proposed (IPCC, 1992), and a multitude of general circulation models (GCMs) have been used to estimate the climate change in the experimental period (Manabe, 1983; Cess et al., 1993; Kacholia and Reck, 1997). Because these scenarios take little account of the biotic feedbacks stemming from the atmosphere-biosphere CO_2 exchange, the Sim-CYCLE simulation is expected to give an approximation of the potential feedback effect. Finally, the potential role of the terrestrial ecosystems in the global biogeochemical carbon cycle under the changing environment will be discussed.

6.2. Simulation design

6.2.1. Simulation model

Simulation configuration of Sim-CYCLE was similar to that of Chapter 4: spatial resolution of 0.5°x0.5° longitude-latitude, and calculation time-step of one month. The soil data and long-term mean climate data were derived from the same sources to the equilibrium run (cf. Chapter 4). The Olson's biome mapping was also adopted, but for convenience, it was assumed that the movement of biome (and C_3/C_4 composition) is negligible during the experimental period of 70 years. This assumption of stationary biome may be appropriate, because grid-to-grid distance (i.e. 55 km) is sufficiently lengthy in the light of the velocity of biome shift. For each grid cell, at first, equilibrium carbon dynamics was attained in the same manner to the equilibrium run in Chapter 4, and subsequently climate change projection (see next section) was incorporated for capturing the transitional change in the carbon dynamics.

6.2.2. Global environmental change

Sensitivity analysis. At first, a sensitivity analysis is performed to clarify the sensitivity of the biospheric carbon dynamics. The transitional changes in *NPP* and *NEP* are simulated, in response to step-wise environmental changes: atmospheric CO_2 doubling from 353 to 707 ppmv, global warming by 3 °C, and precipitation increased by +30%.

Climate change scenario. In this study, climate scenarios by three GCMs were adopted: the U.S. Geophysical Fluid Dynamics Laboratory (GFDL; Manabe et al., 1991, 1992), the U.S. Goddard Institute for Space Studies (GISS; Russel et al., 1995), and Japan Meteorological Research Institute (MRI; Tokioka et al., 1995). They are all coupled atmosphere-ocean models, with minor differences in spatial resolution and parameterization schemes. These three climate projection scenarios on the assumption that atmospheric CO_2 concentration increases at a rate of +1% yr^{-1} are termed the GFDL case, the GISS case, and the MRI case, respectively. In addition to the three scenarios using the same configuration but different models, two supplementary scenarios were derived from the MRI-GCM. One scenario takes the effect of anthropogenic sulfate aerosols into account, because their optical perturbation can affect the future projection of the global warming (Haywood et al., 1997; Mitchell and Jones, 1997); the scenario is termed the MRIs case. Another scenario assumes a halved rate of the atmospheric CO_2 growth, i.e. +0.5 % yr^{-1} and is termed the MRIh case. Indeed, this halved rate seems more plausible, compared with the contemporary CO_2 growth rate (+0.45 % yr^{-1}) (Gray, 1998). In each GCM scenario, climate change was represented by the variations in temperature and precipitation, between the control run (without CO_2 change) and the experimental run (with CO_2 change). Along with the precipitation change, solar radiation can be affected by the variation in cloud cover, but the effect will be explored in the future.

Atmospheric CO_2 concentration At first, atmospheric CO_2 concentration was fixed to 352 ppmv, the level in 1990, until the equilibrium state is obtained (long-term mean climate is used at this stage). Then, atmospheric CO_2 is increased at a rate of +1 % yr^{-1}, in a compound manner, up to 707 ppmv in the 70th year (GFDL, GISS, MRI, and MRIs scenarios). As a reference case, a simulation assuming the sole gradual CO_2 doubling

($2xCO_2$) was performed. In case of the MRIh scenario, the halved rate of +0.5 % yr^{-1} was adopted; atmospheric CO_2 concentration reaches 500 ppmv at the 70th year. Then, the prediction run may account for the transitional environmental change from AD 1990 to 2060, using a few simplifying assumptions.

6.3. Result 1: sensitivity analysis

The step-wise environmental changes resulted in apparently changed *NPP* with little time-lag in responsiveness (Fig. 6-1a). The CO_2 doubling increased *NPP* from 61.8 to 75.2 Pg C yr^{-1} in as early as the second year of the simulation, and the increased precipitation by 30% also increased *NPP* to 67 Pg C yr^{-1}. However, the global warming by 3°C did not induce large *NPP* change: 62.5 Pg C yr^{-1} at the 70th year. A distinctive situation was revealed for the *NEP* transition (Fig. 6-1b). The warming resulted in a net carbon emission (*NEP*<0) of as much as 14 Pg C yr^{-1} at the first year, which diminished gradually but continued over 70 years. In contrast, CO_2 doubling and precipitation increase resulted in positive *NEP*s. It is important that the estimated *NEP*s induced by CO_2 doubling and warming by 3 °C are opposite in direction but comparable in magnitude.

6.4. Result 2: prediction with 3 GCM scenarios

6.4.1. Climate change

Along with the increase of atmospheric CO_2 concentration, global mean land temperature rose approximately linearly independent of the GCMs adopted (Fig. 6-2a). The magnitude of the temperature change seems comparable between the three GCMs, but GFDL one was slightly higher (+2.5 °C at 61-71th years) than others (+1.9 to +2.1 °C). The warming was remarkably heterogeneous over the land surface (Fig. 6-3), such that northern high latitudinal zones would undergo more severe temperature change typical for the GCM simulations of global warming (e.g. Manabe, 1983; Schlesinger and Mitchell, 1987). Precipitation variation was more changeable between years and between GCMs (Fig. 6-2b). The MRI scenario suggests the large increase of precipitation in Monsoon Asia, central Africa, and northern Eurasia (Fig. 6-3), while GISS one suggests, in stead, an approximately stable amount of precipitation.

6.4.2. Overview of carbon dynamics change

Global *NPP* was estimated to increase significantly in all GCMs, as a result of global environmental change (Fig. 6-4a). Sole CO_2 doubling resulted in *NPP* of 74.6 Pg C yr^{-1}, or +21.0 % of the contemporary one. Interestingly, CO_2 doubling coupled with climate change resulted in larger *NPP*s after the ca. 30th year: 77.9 to 79.9 Pg C yr^{-1}, or +26.4 to +29.8 %, in the 61-70th years. These fertilization effects correspond to the biotic growth factor (β; Kohlmaier et al., 1989; Polglase and Wang, 1992) of 0.38 to 0.43, which is larger than the sole 2xCO_2 one, i.e. 0.30.

$$NPP_{70th} = NPP_{0th}\left[1 + \beta \cdot \ln\left(\frac{CD_{ATM,70th}}{CD_{ATM,0th}}\right)\right] \qquad (6\text{-}1)$$

Mainly due to the increased productivity, biospheric *NEP* was apt to keep positive during the experimental period, except for the first 12 years (Fig. 6-4b). Cumulative annual *NEP* indicates the net response of the biosphere to the prescribed environmental change; +205.8, +74.4, +123.0, and +127.7 Pg C for the sole 2xCO_2, GFDL, GISS, and MRI scenario, respectively. Along with the global change, average *LAI* increased 18 %, or from 2.3 to 2.7, leading to an improvement of radiation use efficiency (data not shown).

The carbon storage in plant and soil compartments changed in a disparate manner, in case of the GCM scenarios (Fig. 6-5). Plant biomass increased to the extent similar to the sole 2xCO_2 case, and discrepancy among the GCM scenarios appears to be small: ΔWP=+114 to +121 Pg C after 70 years. In contrast, the trajectories of soil carbon storage based on GCM climate scenarios were disparate from the 2xCO_2 case, in which as much as 98 Pg C was sequestered into the soil carbon storage. In the GISS scenario, soil carbon storage kept an equal level throughout the experimental period (ΔWS=+8.3 Pg C). The MRI scenario predicted a decrease of soil carbon by -10 Pg C during the period from the 10th to 60th year, but resulted in a small increase by +6.6 Pg C at the end of the simulation. The monotonously decreasing trend of the GFDL scenario (ΔWS=–40.2 Pg C at last) is astonishing, because increased plant biomass should increase litterfall, or the carbon supply to soil. Figure 6-6

summarizes the global carbon cycle at the final stage of the 66-70th years, and it can be seen that the net balance of soil carbon (=*LF-HR*) was surely negative in the GFDL scenario, probably because of the strongest impact of global warming on decomposition.

The changes in *NPP* and carbon storage did not take place homogeneously over the terrestrial biosphere, as shown in Figs. 6-7 and 6-8. As a result of sole CO_2 doubling, *NPP* in such subtropical regions as eastern Africa, India and southern Australia responded largely. Ecosystem carbon storage increased in many regions, especially in humid tropical regions (Fig. 6-7). The large carbon accumulation to tropical ecosystems was attributable to increased plant carbon storage, while moderate sequestration in temperate and boreal regions resulted from increased soil carbon storage (Fig. 6-8). Taking account of climate change, distribution of *NPP* enhancement changed in many regions. *NPP* increased largely in eastern Africa in each of the three GCM scenarios, while the increase in Australia and India was not conservative. In stead, a part of central America and eastern Siberia showed large *NPP* stimulation. In such arid regions as North Africa and central Asia, *NPP* decreased to some extent. The large carbon accumulation into tropical ecosystems (sole $2xCO_2$ case) was diminished in a majority of grid cells, and some boreal ecosystems, especially southern Siberia in the GFDL scenario (Fig. 6-7), released carbon to the atmosphere. Nevertheless, other part of the boreal ecosystems acted as a strong carbon sink (e.g. Alaska and northern part of Siberia). In the MRI scenario, Sahelian region absorbed a large amount of carbon. The boreal ecosystems underwent two opposite effects by climate change, i.e. augmentation of biomass and reduction of soil carbon storage (Fig. 6-8).

6.4.3. Biome specific aspects

As shown in Fig. 6-9, *NPP* change was not equal among the 32 biome types. Compared with the average of +21 %, semiarid woodlands (biome 6), Mediterranean-type dry woodlands (biome 17), hot and warm wetlands (biome 23), and irrigated croplands (biome 29) showed larger *NPP* increase (>40 %) as a result of CO_2 doubling. In contrast, main deciduous boreal forests (biome 10), tundras (biome 21), and wooded tundras (biome 22) showed smaller *NPP* increase (<10%). (The small CO_2 fertilization effect in tundra ecosystems seems consistent with observations (Grulke et al., 1990; Mooney, 1991; Körner,

1993)). The climate change exerted little effect on tropical forest *NPP*, while it enhanced *NPP*s in northern deciduous taiga (biome 12), Tibetan meadows and Siberian highlands (biome 20), tundras, wooded tundras, and cool bogs and mires (biome 24). Figure 6-10 shows the frequency distribution of *NPP* change as a result of 70-year global change, for each scenario. The modes of distributions are different with or without the climate change; in contrast to a single peak of the $2xCO_2$ case, there was the second peak around +20 %, made mostly by the occurrence of forest grid cells (biomes 1-12). (The 20 % increase of *NPP* seems typical for a wide variety of woody species (Ceulemans and Mousseu, 1994; Wullschleger et al., 1995; Curtis and Wang, 1998; Norby et al., 1999)). The impact on carbon storage was also different among the biome types (Fig. 6-11). The large carbon uptake (ΔWE) into tropical rain forest (biome 1), estimated by the sole $2xCO_2$ case, was decreased by climate change, from 43 Pg C to 25 Pg C; especially, carbon uptake into soil was almost completely canceled. The large *NPP* enhancement of semi-arid woodlands (biome 6) did not result in large carbon sequestration in any scenarios. The loss of soil carbon from temperate and boreal forests (biomes 4 to 12) is notable; main evergreen taiga (biome 9) was estimated to act as a net carbon source in the GFDL scenario. On the other hand, a large amount of carbon was sequestered as soil organic matter in warm grasslands (biome 19).

The response to the global environmental change was different between C_3 and C_4 plants (Fig. 6-12), because C_3 plants were assumed to be more sensitive to atmospheric CO_2 level (cf. Table 2-1). Of the 12.9 Pg C yr^{-1} of total *NPP* increase induced by CO_2 doubling, 85.8 % was by C_3 plants and the remnant was by C_4 plants; this implies that the contribution of C_4 plants to total *NPP* was reduced from 20.3 % to 19.2 %. The GFDL and MRI scenarios estimated similar decreases of the C_4 plant contribution (18.7 and 19.6 %, respectively), while the GISS scenario expected the same magnitude of C_4 contribution (20.2 %).

6.4.4. Latitudinal aspects

The spatial heterogeneity in the responses of terrestrial carbon budget (cf. Figs. 6-7 and 6-8) may become comprehensive by aggregating into latitudinal zones. Figure 6-13 shows the time-series of the carbon storage change along with 5°-composite zones. In the sole $2xCO_2$ case, a majority of carbon uptake was concentrated around the equator; there was no

source zone throughout the simulation period. When the climate scenarios were incorporated, northern high latitudes around 60°N acted as strong carbon sources from the 20th to 30th year, and net sinks around the equator were reduced after the ca. 50th year.

The latitudinal distribution of *NPP* change (Fig. 6-14) represents the difference of responsiveness among latitudinal zones. The sole CO_2 doubling enhanced *NPP* chiefly in lower latitudinal zones, whereas incorporating the GCM scenarios resulted in larger stimulation of *NPP*s in middle to high latitudinal zones. In the latitudinal zones from 40°N to 80°N, the increment of *NPP* was +3.3 Pg C yr^{-1} in the sole $2xCO_2$ case, but +5.8 to +8.3 Pg C yr^{-1} in the climate change cases. In consequence, plant biomass in the northern zones gained a larger amount of carbon (Fig. 6-15), although they lost a comparable amount of soil carbon. In other words, the ratio of plant/soil carbon pools shifted close to that of lower latitudes; the contemporary ecosystems in the northern regions have lower plant/soil carbon storage ratio than tropical zones (cf. Fig. 4-8). If this deduction is true, the soil carbon loss is not an instantaneous but an inevitable consequence of the global warming.

6.5. Result 3: prediction with 3 MRI-GCM scenarios

6.5.1. Climate change

Based on the different assumptions of environmental change, the MRI-GCM provided a set of different climate scenarios, i.e. MRI, MRIs, and MRIh (Fig. .6-16). Compared with +2.1°C in the MRI scenario (the 70th year), MRIs and MRIh gave lower estimations of the global warming: +1.6°C and +1.0°C, respectively. In the MRIh scenario, many regions would experience only a small degree of warming (Fig. 6-17). The precipitation of the MRIs and MRIh scenarios showed increments, however, to less extent (Fig. 6-16). No consistent difference in the precipitation pattern was found among the three MRI-GCM scenarios.

6.5.2. Carbon dynamics change

Through the simulation period, *NPP* of the MRI case was larger than the MRIs one (Fig. 6-18), but the difference between them was small (<1 Pg C yr^{-1}). And, *NPP* of the MRIh case was apparently smaller than other two cases, certainly due to the lower atmospheric CO_2

concentration. Nevertheless, the biotic growth factor β of the MRIh case, 0.432, was larger than those of the MRI (0.428) and MRIs (0.389). The estimated *NEP*s were not significantly different between the MRI and MRIs, but the MRIh scenario resulted in smaller uptakes. Finally, the 70-year cumulative *NEP* of the MRIs case was 124.0 Pg C, which is comparable to the MRI one (127.7 Pg C), and a larger amount of carbon was sequestered into soil, rather than biomass (Fig. 6-19). Then, although inclusion of the effect of sulfate aerosols improved the reliability of GCMs (Mitchell et al., 1995; Haywood et al., 1997), this may exert little effect on the prediction of terrestrial carbon budget, unless the cloudiness change is included. The MRIh scenario lead to a carbon sequestration into biomass (ΔWP=+50.1 Pg C), which became evident after the 30th year, and to a small emission from soil organic matter (ΔWS=–5.4 Pg C). The total change of +44.7 Pg C is one third of the MRI case. In the MRIs case, larger changes in *NPP* and carbon storage were estimated in basically similar regions to the MRI case (Figs. 6-20 and 6-21): subtropical Africa, Australia, and central South America. These changes were underrepresented by the MRIh case; even in tropical and northern high regions, biomass increase was not so evident. However, soil carbon change occurred to the comparable extent to the MRI and MRIs cases: e.g. increase in Sahelian grasslands and Australian deserts, and decrease in central Siberian taiga.

6.4. Discussion

6.4.1. Atmospheric CO_2 rise and *NPP*

The increased *NPP* (Fig. 6-4) is primarily attributable to the fertilization effect due to the atmospheric CO_2 doubling. Then, is it possible to derive a consistent relationship between the atmospheric concentration and the terrestrial *NPP* at the global scale? Figure 6-22 plots the estimated *NPP* as a function of atmospheric CO_2 concentration (CD_{ATM}), including the effect of climate change. It can be seen from Fig. 6-22 that *NPP* would be underestimated, if the effect of climate change is not included, especially under a higher atmospheric CO_2 concentration. Moreover, it seems that global *NPP* may be deduced using the empirical equation, with an accuracy within ± 2 Pg C yr^{-1} (r^2=0.934):

$$NPP\left(Pg\ C\ yr^{-1}\right) = 43.977 + 0.052597 \cdot CD_{ATM}\left(ppmv\right) \quad (6\text{-}2)$$

Equation 6-2 is based on all the three GCM scenarios; see Fig. 6-22 for the individual regressions. In the light of the fact that there is a considerable difference in *NPP* responsiveness among the biome types and regions, the high convergence of CD_{ATM}-*NPP* relationship deserves particular attention. Nevertheless, *NEP* is strongly dependent on the time passage from the environmental change (cf. Fig. 6-1b), suggesting that a simple regression to environmental factors may not be viable for prediction.

6.4.2. Biotic feedback to global environmental change

The changed carbon fluxes and carbon storage can in turn exert the feedback effect on the first impact, in either a positive or a negative direction. Figure 6-4 indicates that the estimated *NEP*s were almost positive after the 10th year of simulation (i.e. AD 2000), acting as a negative feedback to the global warming induced by the atmospheric CO_2 rise. However, their magnitude of 1 to 3 Pg C yr^{-1} may not fully offset the anthropogenic CO_2 emission of 6 to 20 Pg C anticipated in the next century (IPCC, 1994). Through the simulation period of 70 years, the 5 simulations predicted that the total carbon storage would increase by 44.7 (MRIh) to 127.7 Pg C (MRI) (Fig. 6-23). They are equivalent to 10 - 17 % of the increment of atmospheric carbon, and comparable to the magnitude of the missing sink at present. Based on the sensitivity analysis (Fig. 6-1), sole global warming resulted in a net carbon source to the atmosphere (i.e. positive feedback of 80 to 158 Pg C), but when atmospheric CO_2 rise was taken into account, a negative feedback took place. Then, if climate system is affected by an external forcing except for CO_2 concentration (e.g. solar radiation change), the terrestrial biosphere may exert a positive feedback effect on the changed climate, through the carbon exchange. These contradictory characteristics of the biospheric feedback may have important implications for the stability and variability of the atmospheric system.

6.4.3. Comparison with other predictions and potential uncertainty

Finally, the predictions of *NPP* and carbon storage are compared with other studies: Melillo (1996) using TEM, and Cao and Woodward (1998a) using CEVSA model. Melillo

(1996) adopted the GFDL, GISS, and OSU (U.S. Oregon State University) scenarios, and predicted that terrestrial carbon storage would increase by +190 to +283 Pg C, when atmospheric CO_2 becomes double. The quantitative difference from the Sim-CYCLE estimation (+74 to +128 Pg C) is attributable to their simulation design of the equilibrium carbon storage after the global change. However, there are several similarities between the two studies; (1) carbon uptake was mostly by plant biomass, rather than soil organic matter; (2) increase of soil carbon storage was diminished when including the global warming, compared with the sole $2xCO_2$ case; (3) the largest carbon uptake took place in tropical ecosystems, and (4) a part of boreal soil could act as a net carbon source. On the other hand, it is contrastive to the Sim-CYCLE prediction that the increment of plant biomass was augmented when including the global warming, compared with the sole $2xCO_2$ case, particularly in boreal ecosystems. Because TEM is a coupled C-N dynamics model, enhanced mineralization and availability of N due to the warming may result in better growth in these ecosystems. Cao and Woodward (1998a) adopted the HADCM (U.K. Hadley Centre for Climate Prediction and Research) scenario, and performed a transitional simulation. They predicted the *NPP* increase of +36 % by AD 2070 and positive *NEP* of about 3.2 Pg C yr^{-1} after 2030 (the 40th year in the Sim-CYCLE study). Using the global warming alone, CEVSA model also estimated the net loss of carbon from the biosphere; atmospheric CO_2 rise turned it into a net sink of carbon. These aspects by CEVSA study are similar to the Sim-CYCLE prediction, but there is one significant difference between the two studies. That is, while Sim-CYCLE estimated that total soil carbon would not be increased by the global change, CEVSA expected that soil carbon would largely increase along with the climate change (about +120 Pg C). Determining whether this is attributable to the difference in climate scenario or the difference in model property requires a further research (e.g. Sim-CYCLE simulation using HADCM scenario).

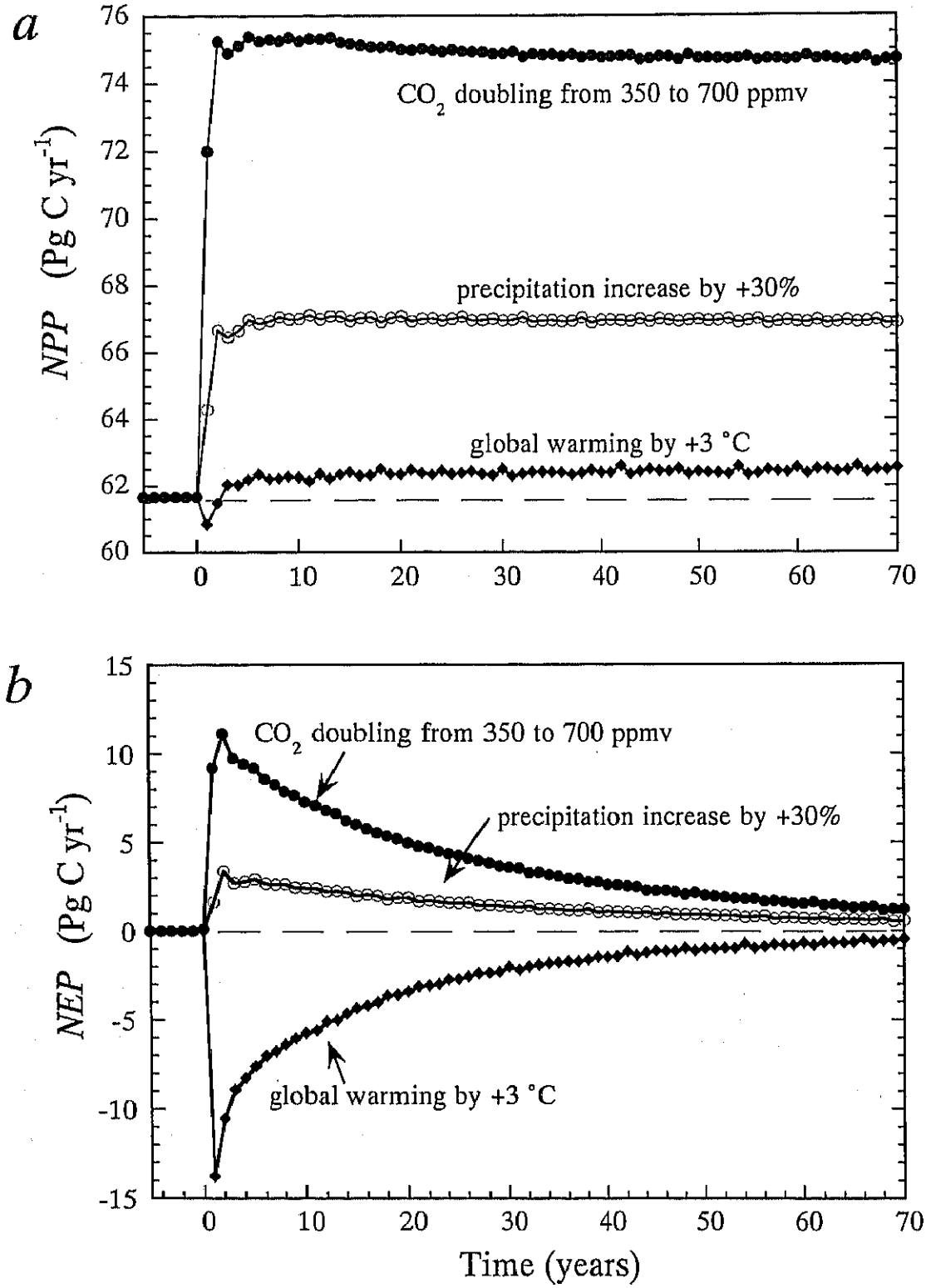

Fig. 6-1. Transitional changes in (a) global *NPP* and (b) global *NEP*, in response to prescribed environmental change.

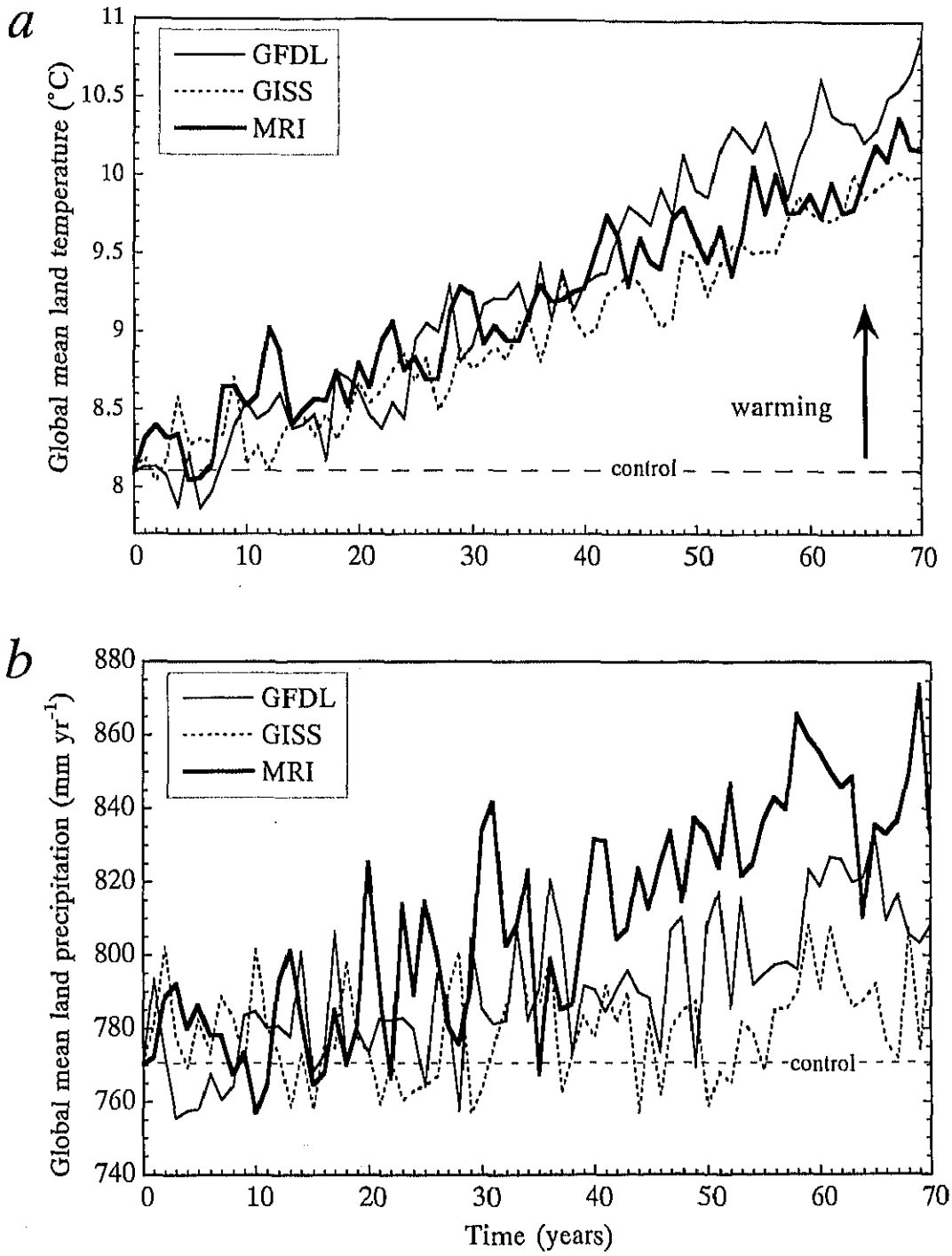

Fig. 6-2. Climate projection by three GCMs (GFDL, GISS, and MRI), on the assumption that atmospheric CO_2 rises by +1 % per year. (a) Global mean land temperature and (b) global mean land precipitation.

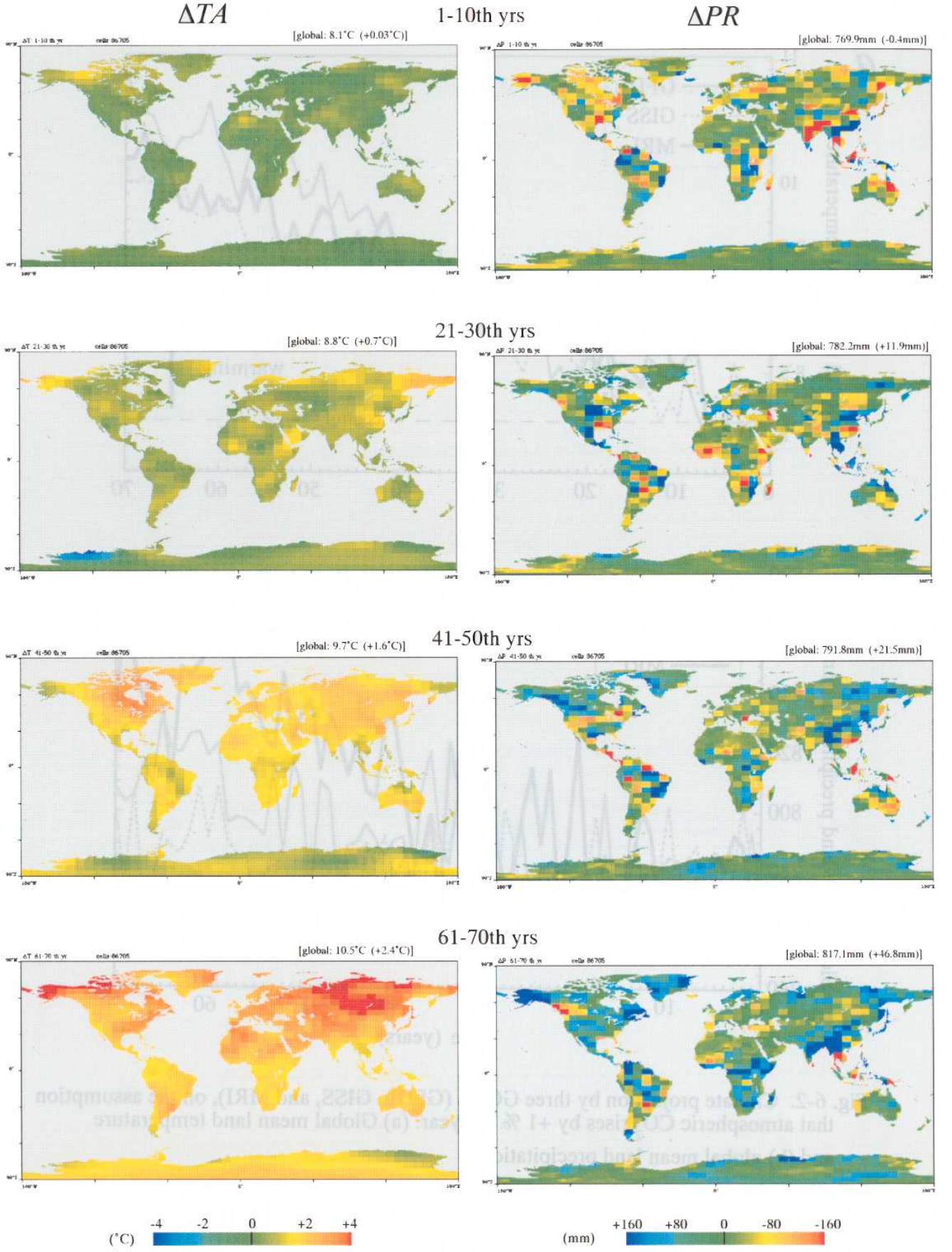

Fig. 6-3. Projected climate change scenarion by GFDL gradual CO_2 doubling simulation.

(GISS scenario)

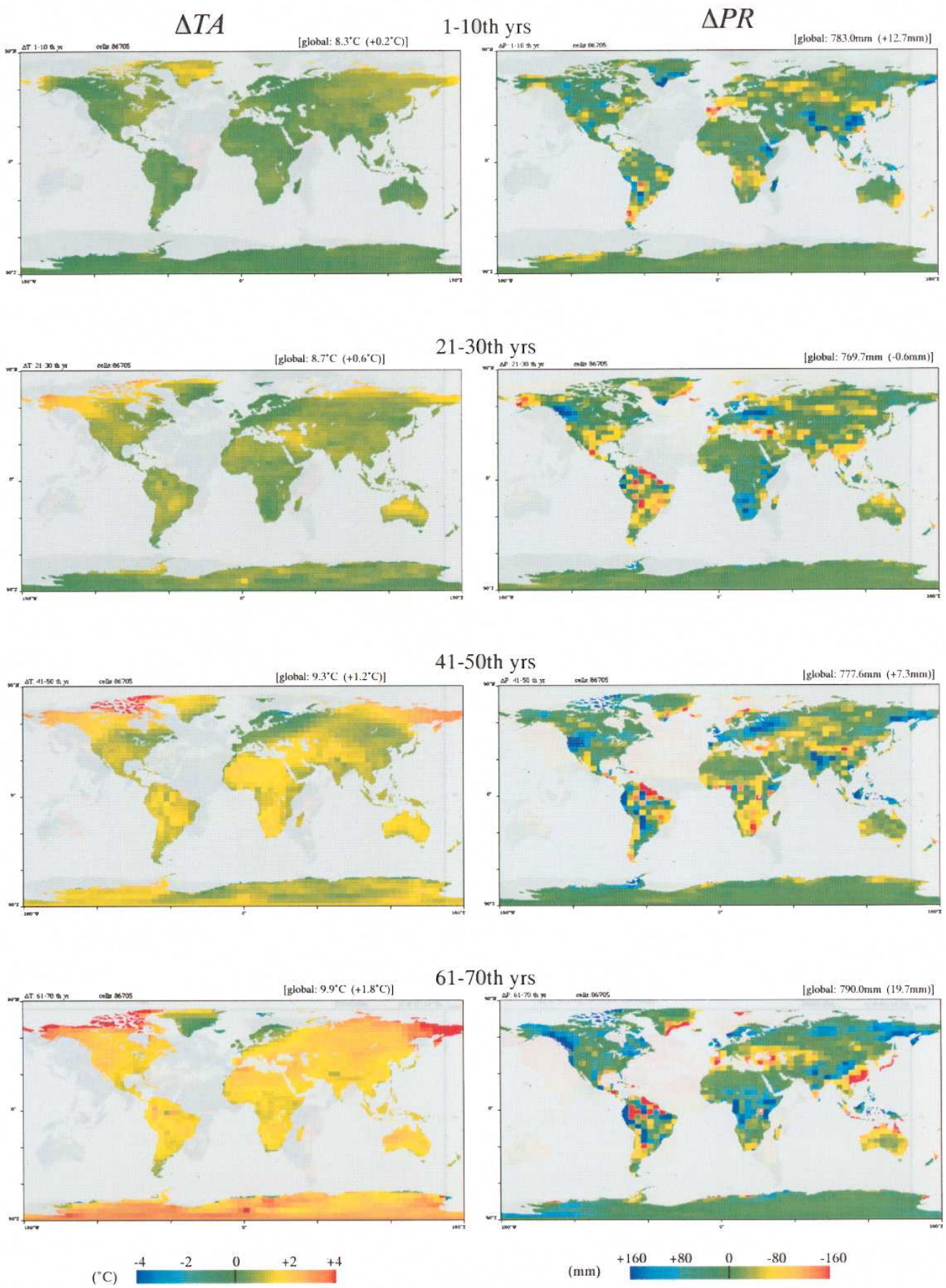

Fig. 6-3(continued). Projected climate change scenarion by GISS gradual CO_2 doubling simulation.

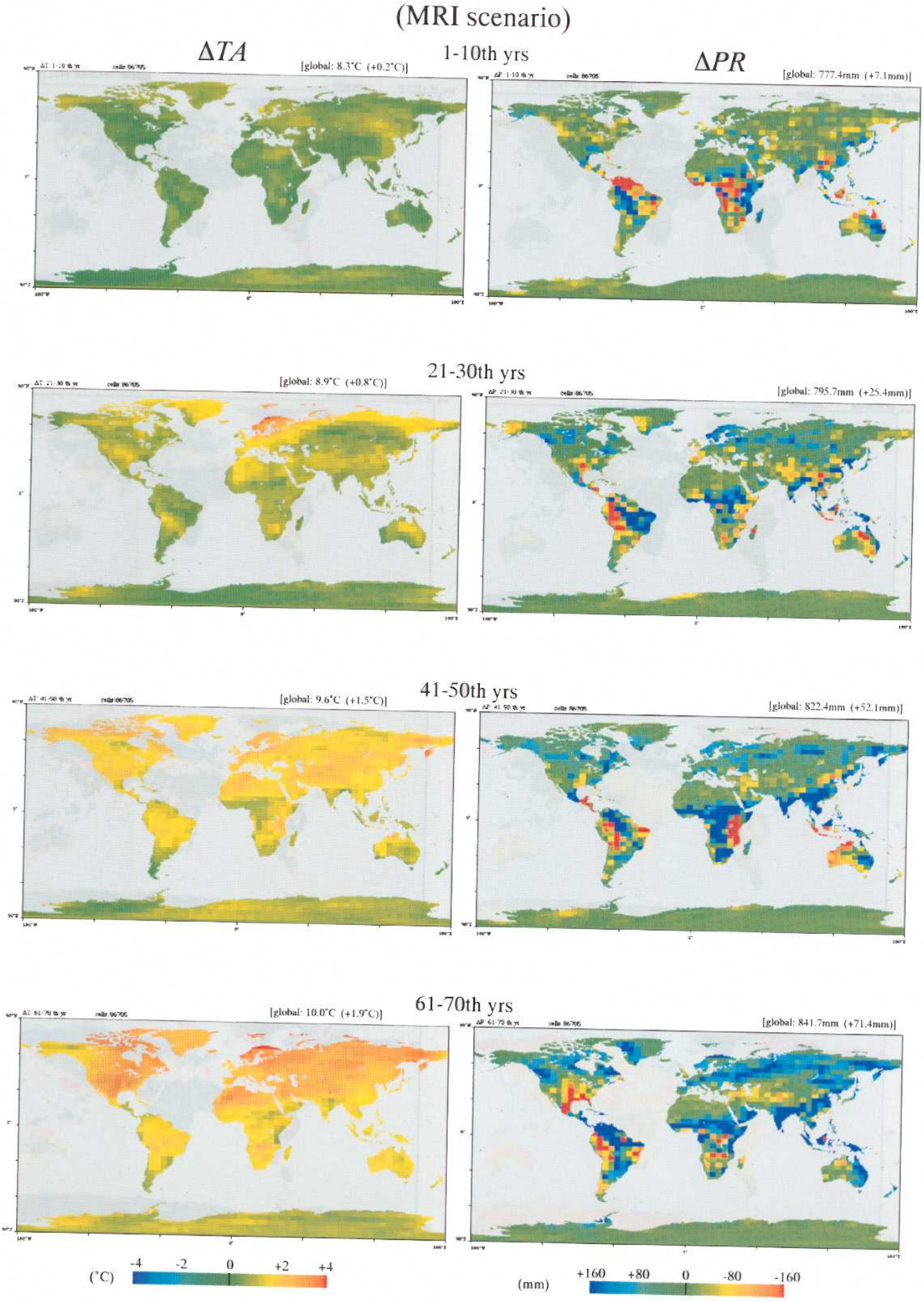

Fig. 6-3 (continued). Projected climate change scenarion by MRI gradual CO_2 doubling simulation.

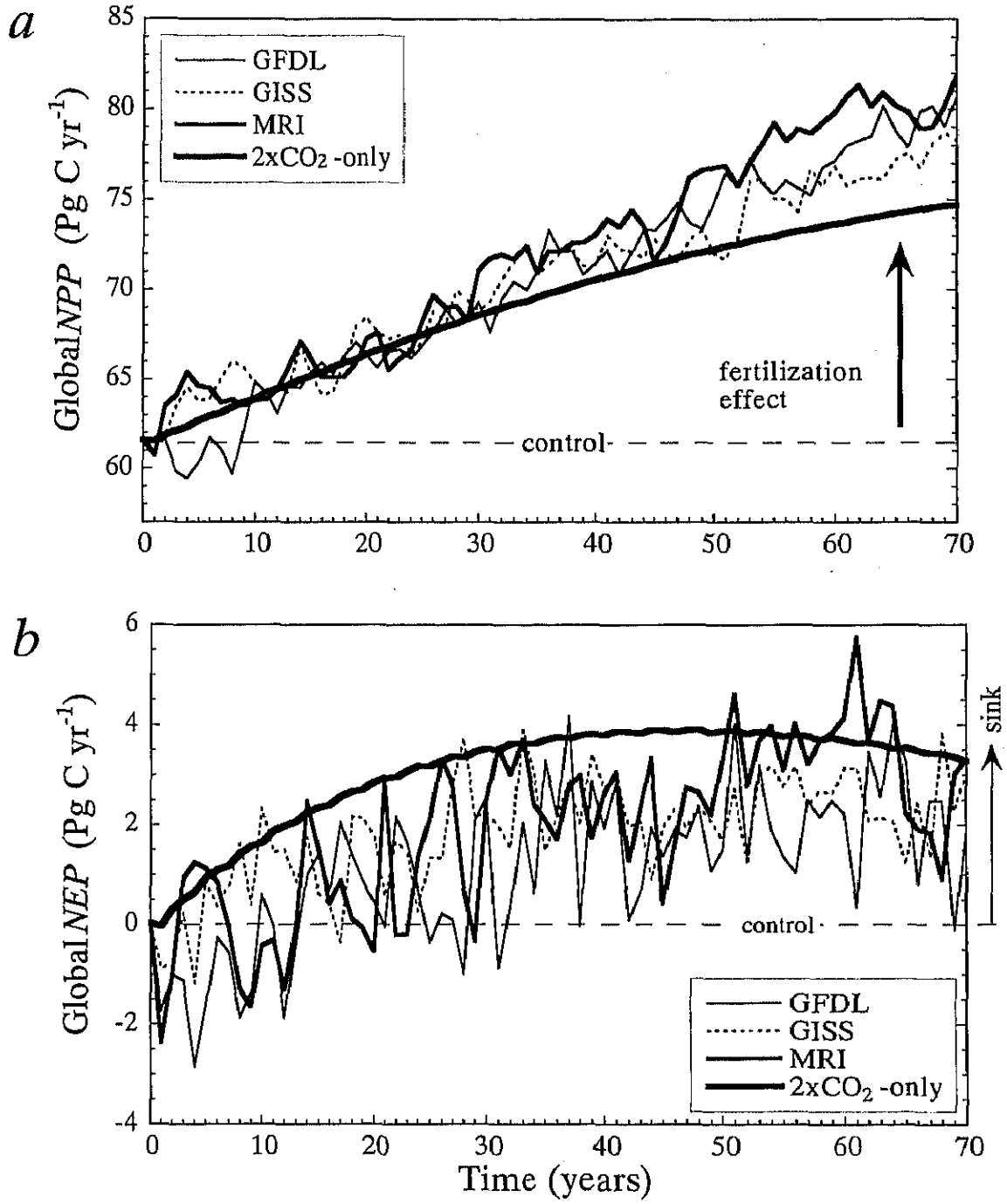

Fig. 6-4. Estimated global NPP and NEP by Sim-CYCLE transient run, using the three GCM climate scenarios.

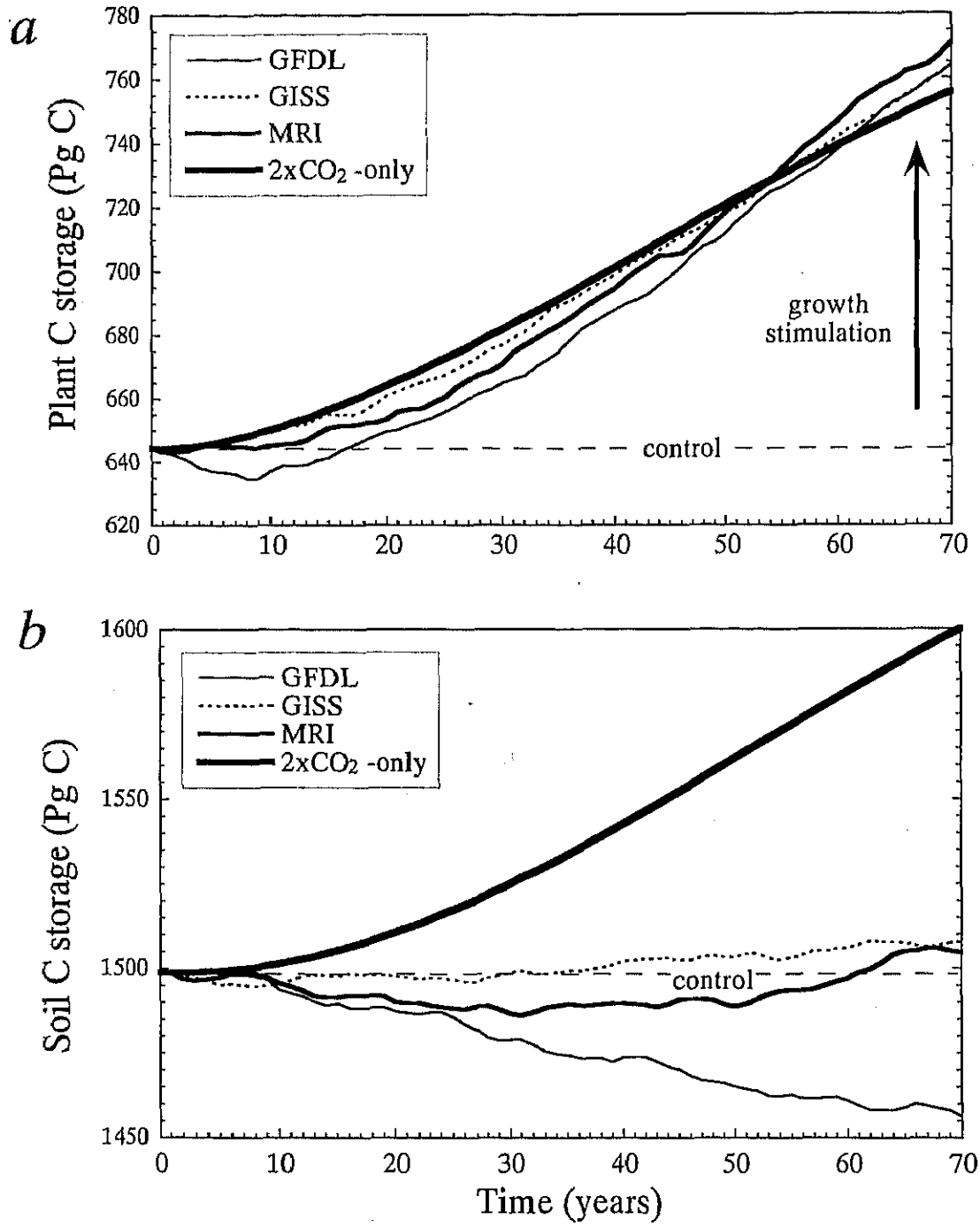

Fig. 6-5. Estimated change in (a) plant carbon storage and (b) soil carbon storage.

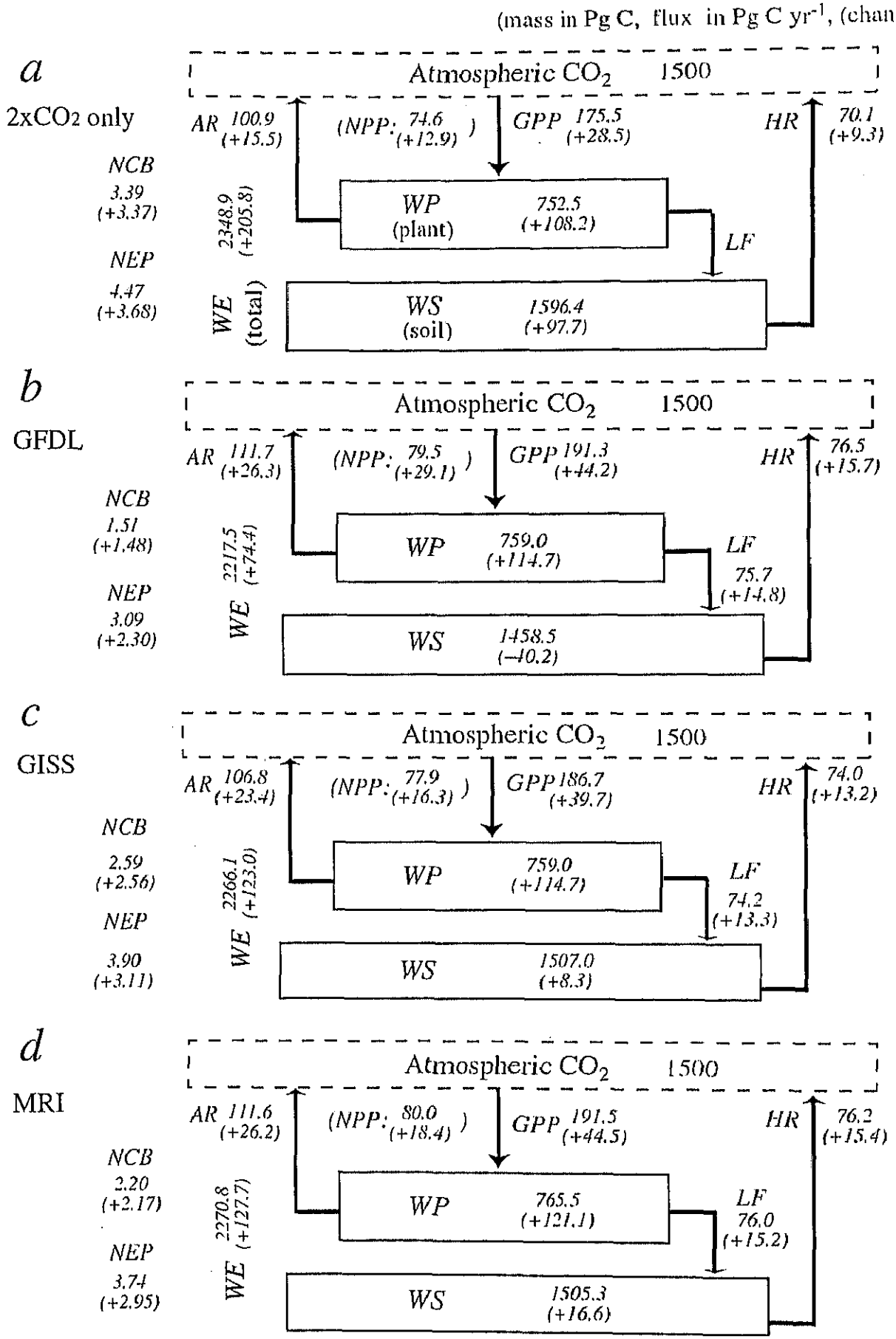

Fig. 6-6. Biospheric carbon dynamics estimated by Sim-CYCLE prediction run, in case of (a) CO_2 doubling only, and (b) GFDL, (c) GISS, and (d) MRI scenarios.

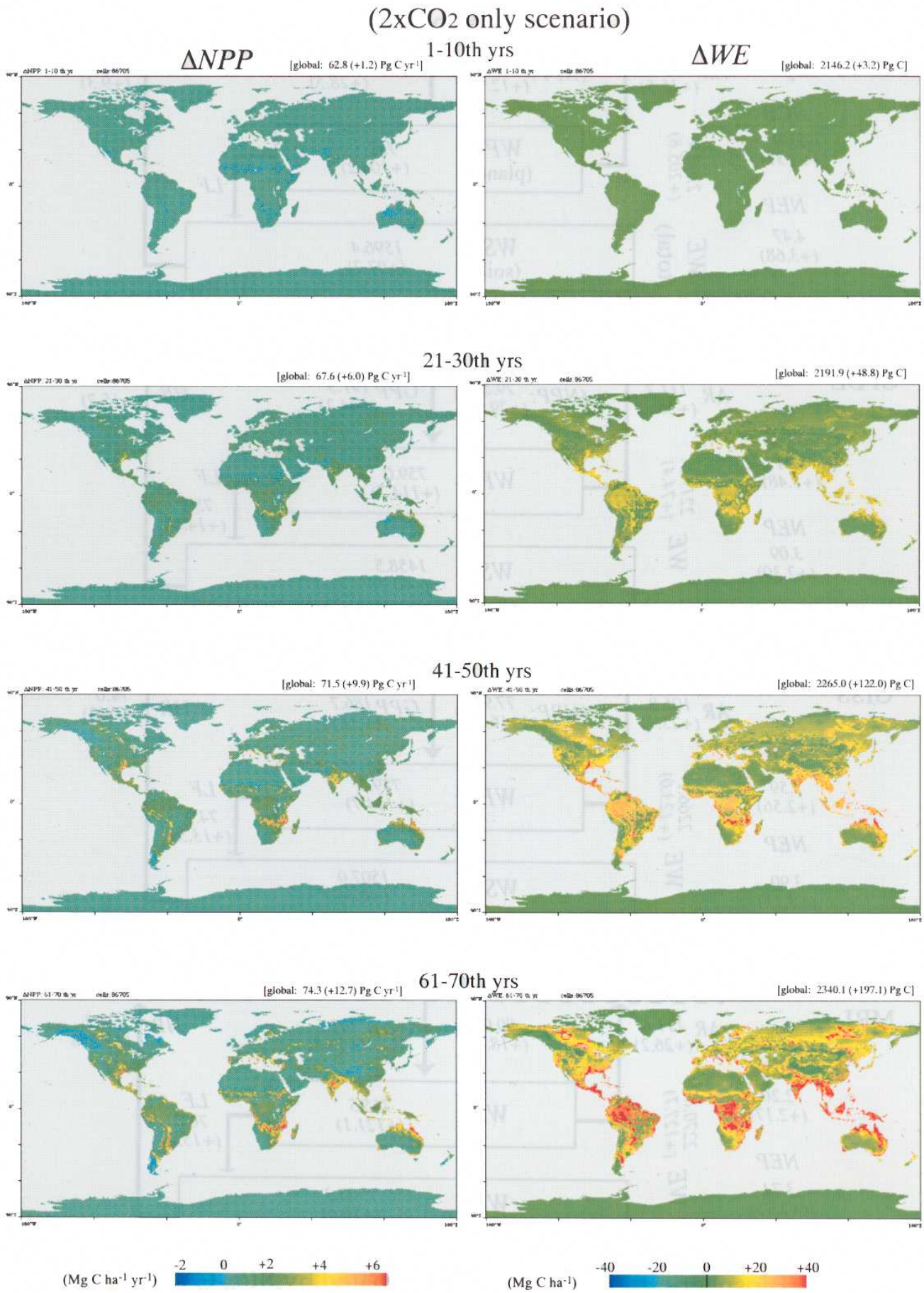

Fig. 6-7. Estimated changes in (left) *NPP* and (right) carbon storage *WE*, under the present climate with gradual CO_2 doubling.

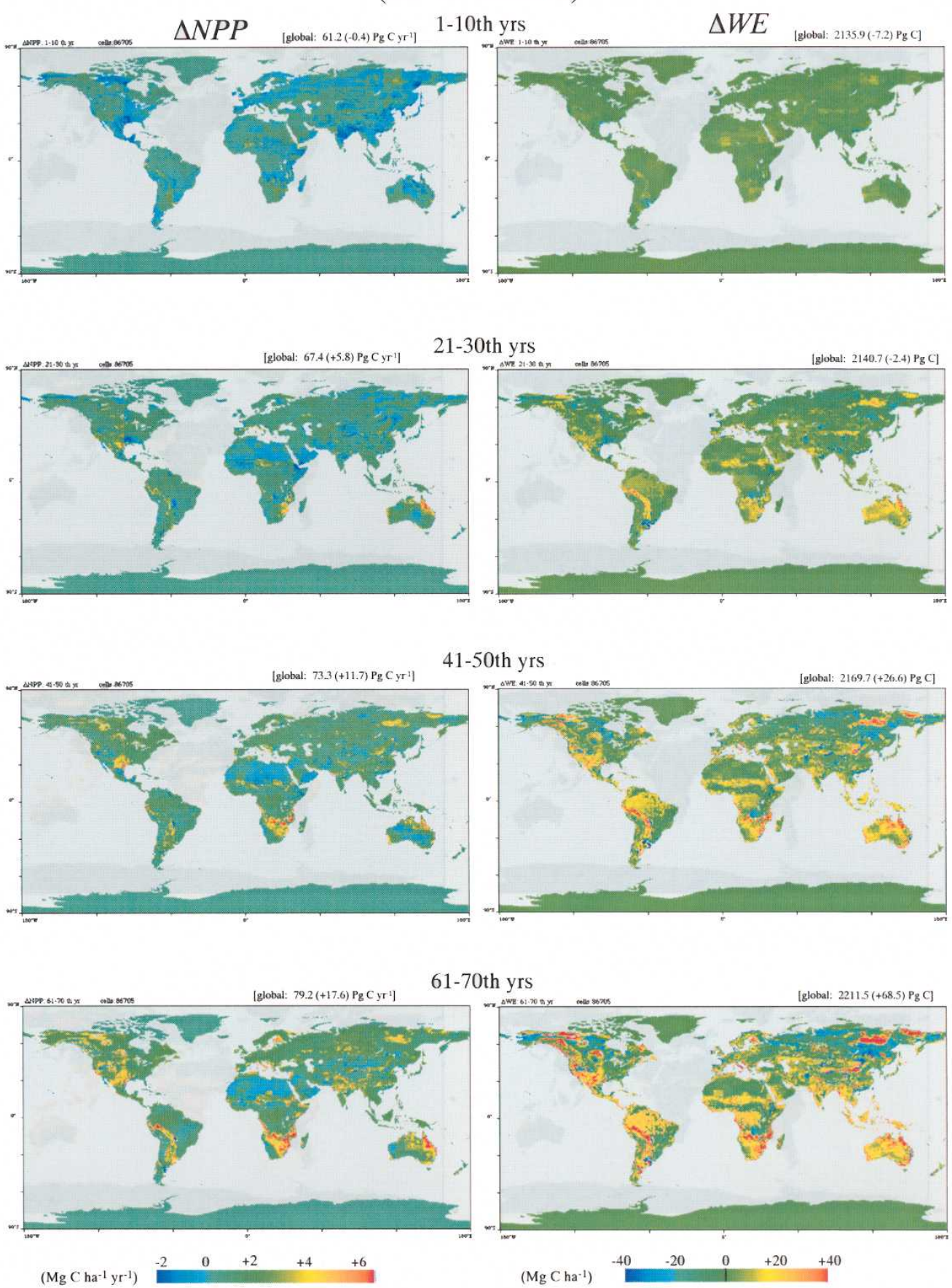

Fig. 6-7 (continued). Estimated changes in (leaf) *NPP* and (right) carbon storage *WE*, under GFDL climate projection with gradual CO_2 doubling.

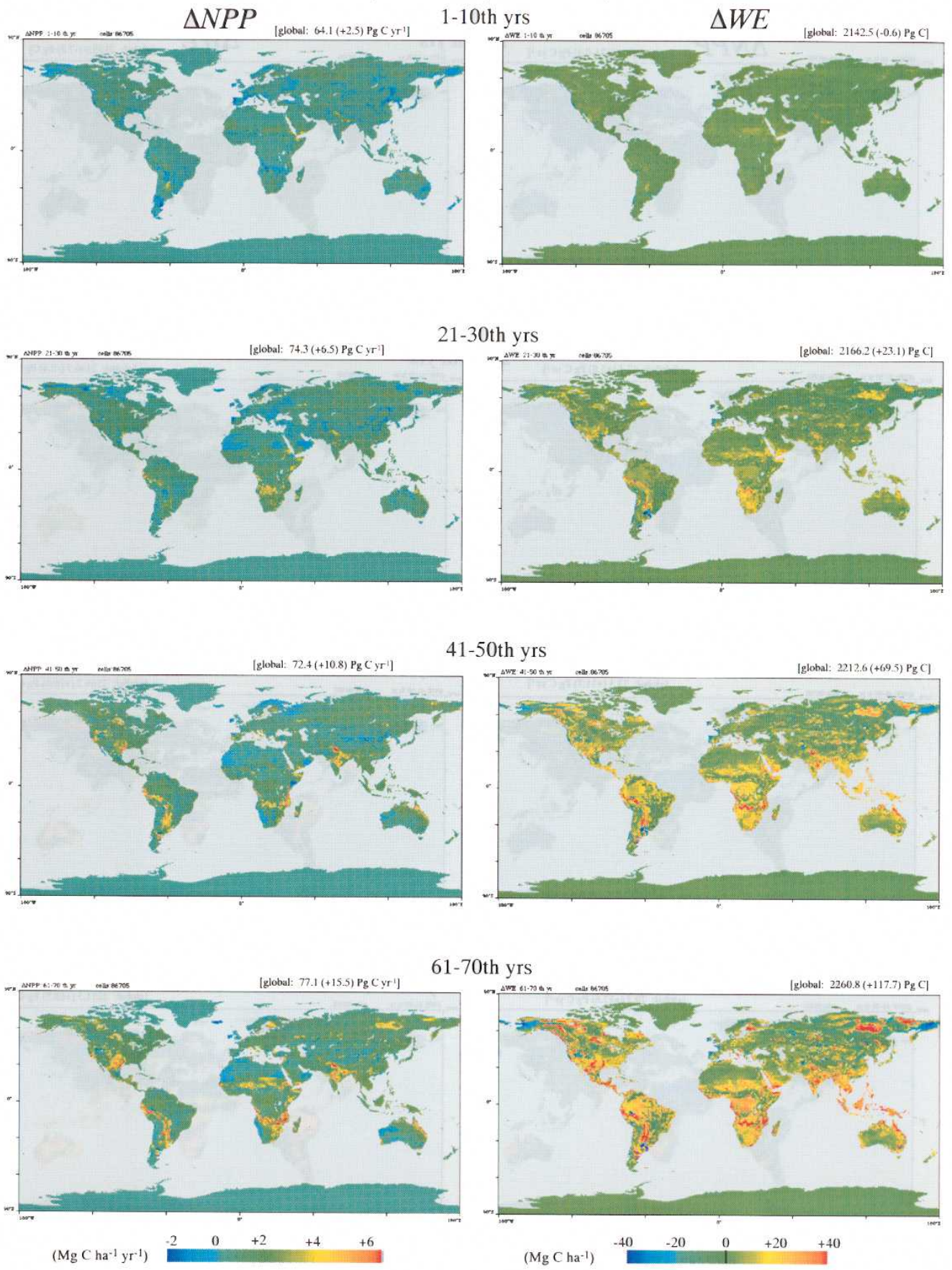

Fig. 6-7 (continued). Estimated changes in (left) *NPP* and (right) carbon storage *WE*, under GISS climate projection with gradual CO_2 doubling.

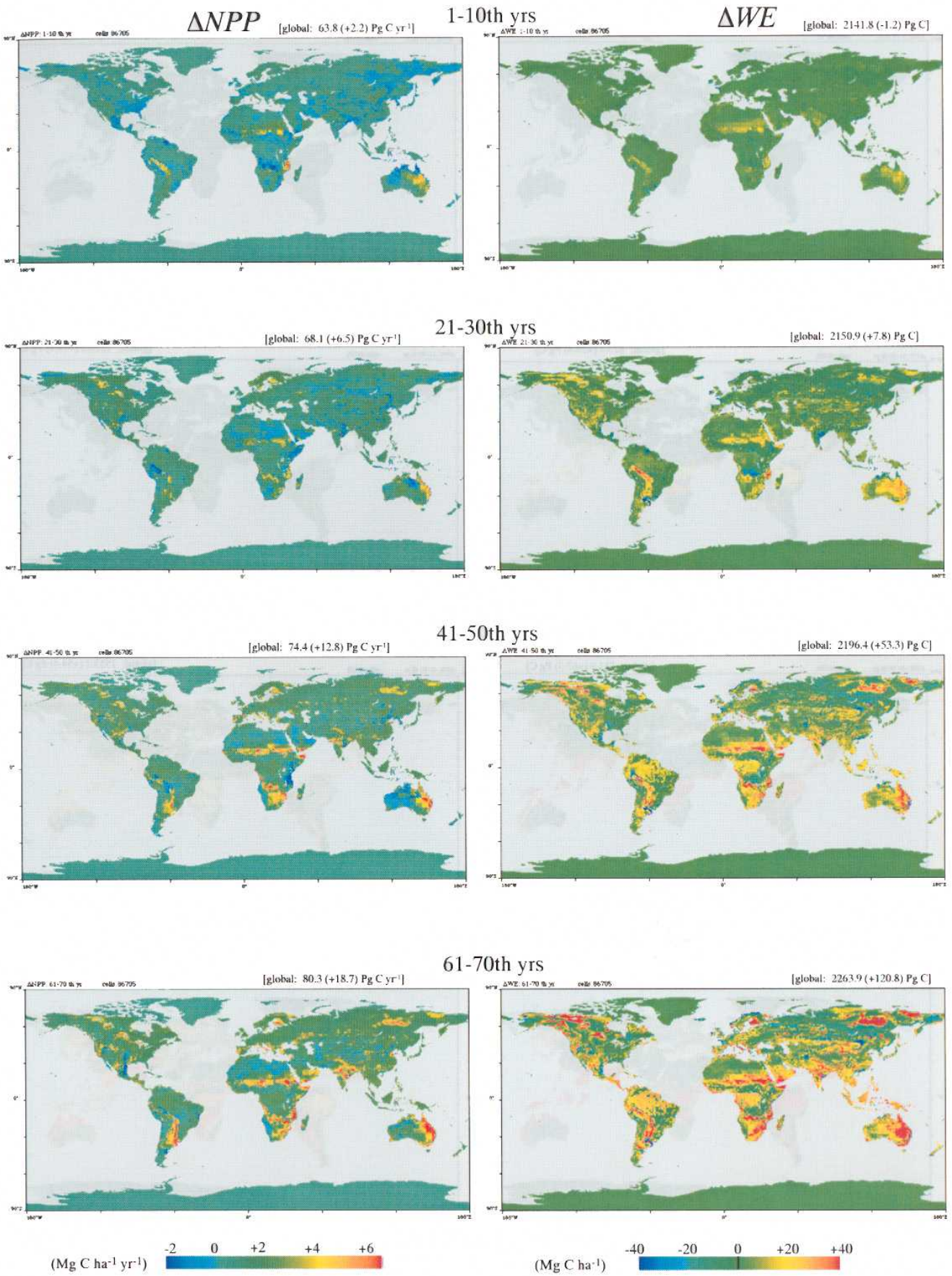

Fig. 6-7 (continued). Estimated changes in (left) *NPP* and (right) carbon storage *WE*, under MRI climate projection with gradual CO_2 doubling.

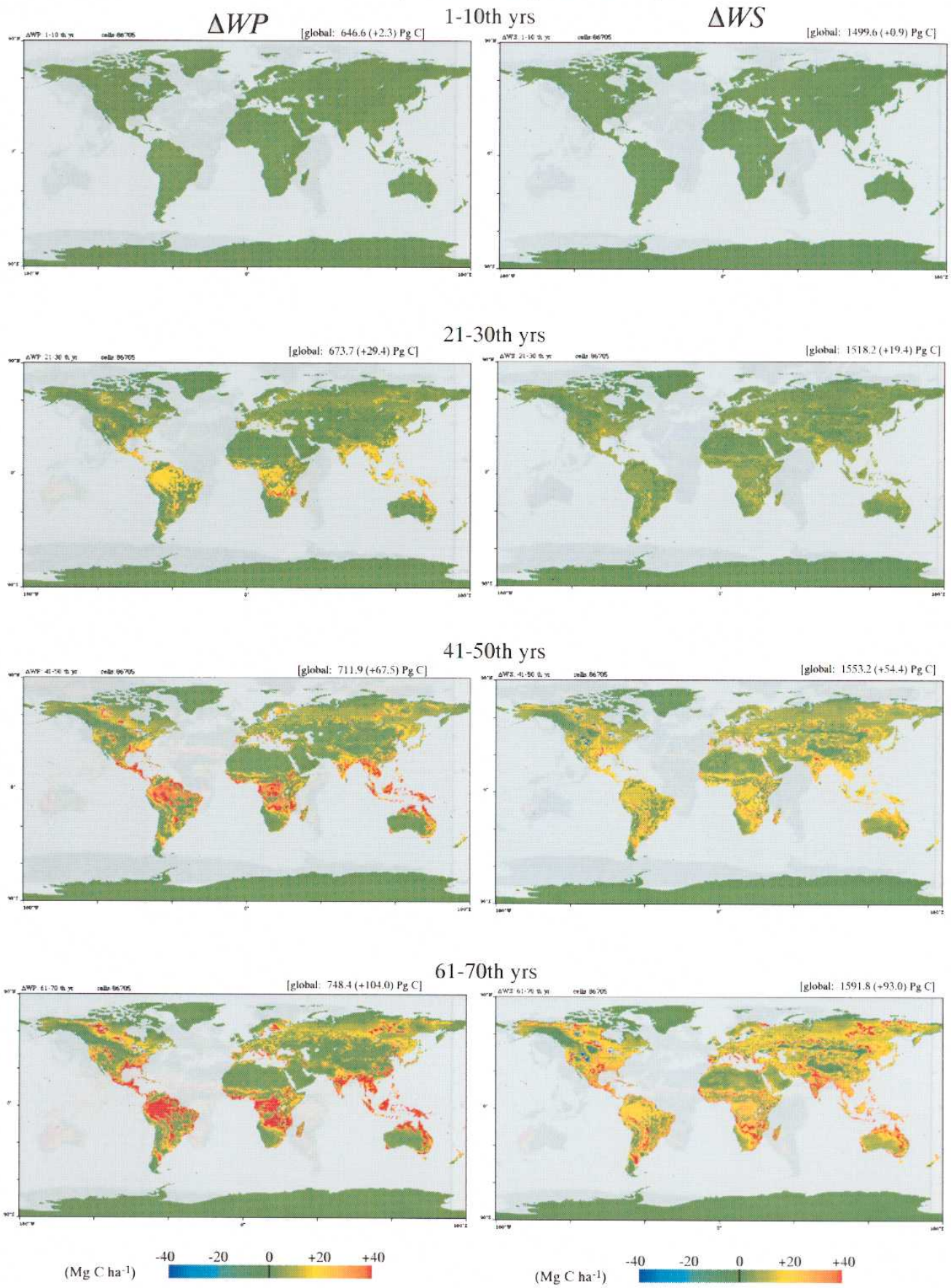

Fig. 6-8. Estimated changes in (left) plant carbon storage *WP* and (right) soil carbon storage *WS*, under the present climate with gradual CO_2 doubling.

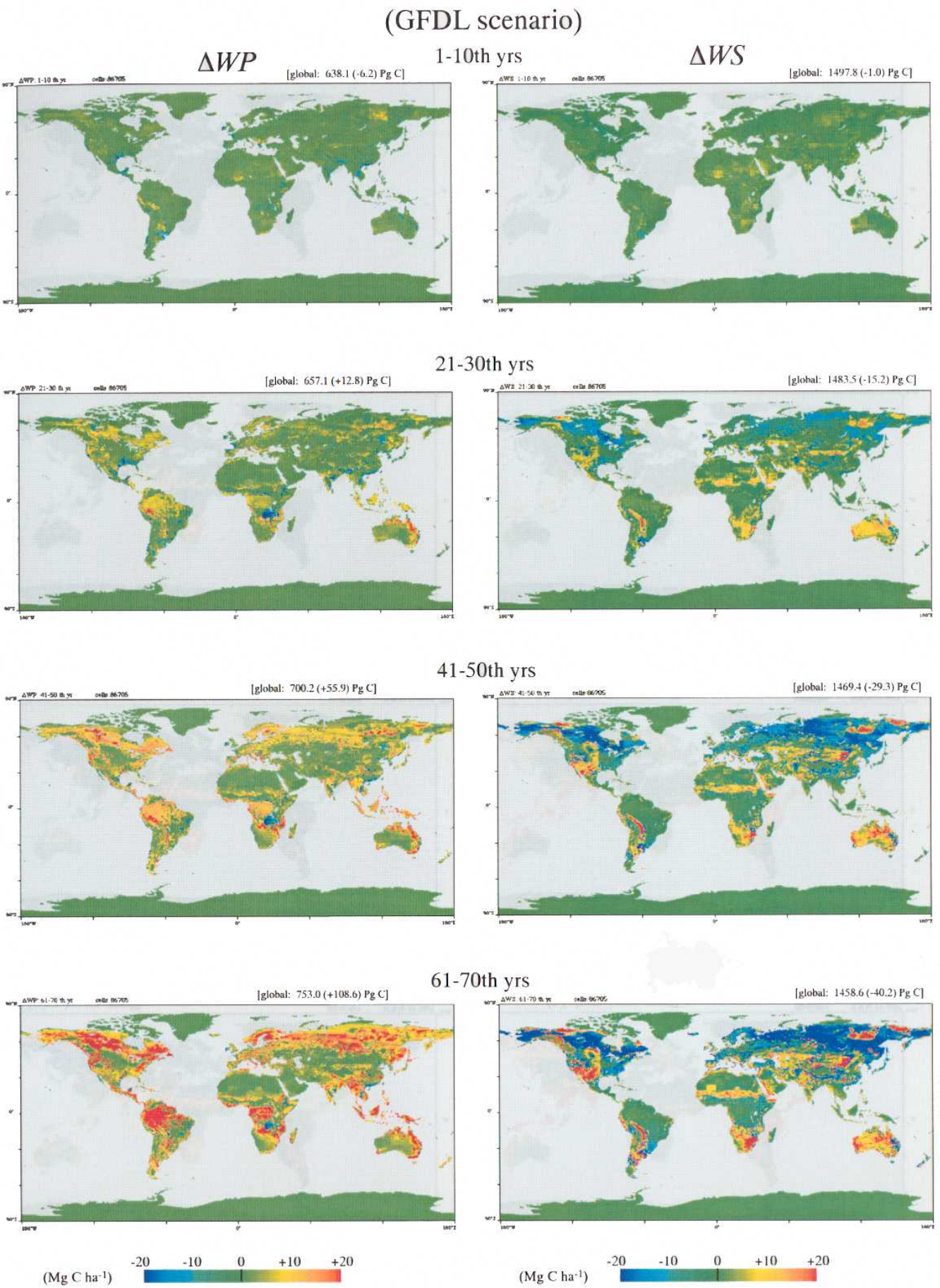

Fig. 6-8 (continued). Estimated changes in (left) plant carbon storage *WP* and (right) soil carbon storage *WS*, under GFDL climate projection with gradual CO_2 doubling.

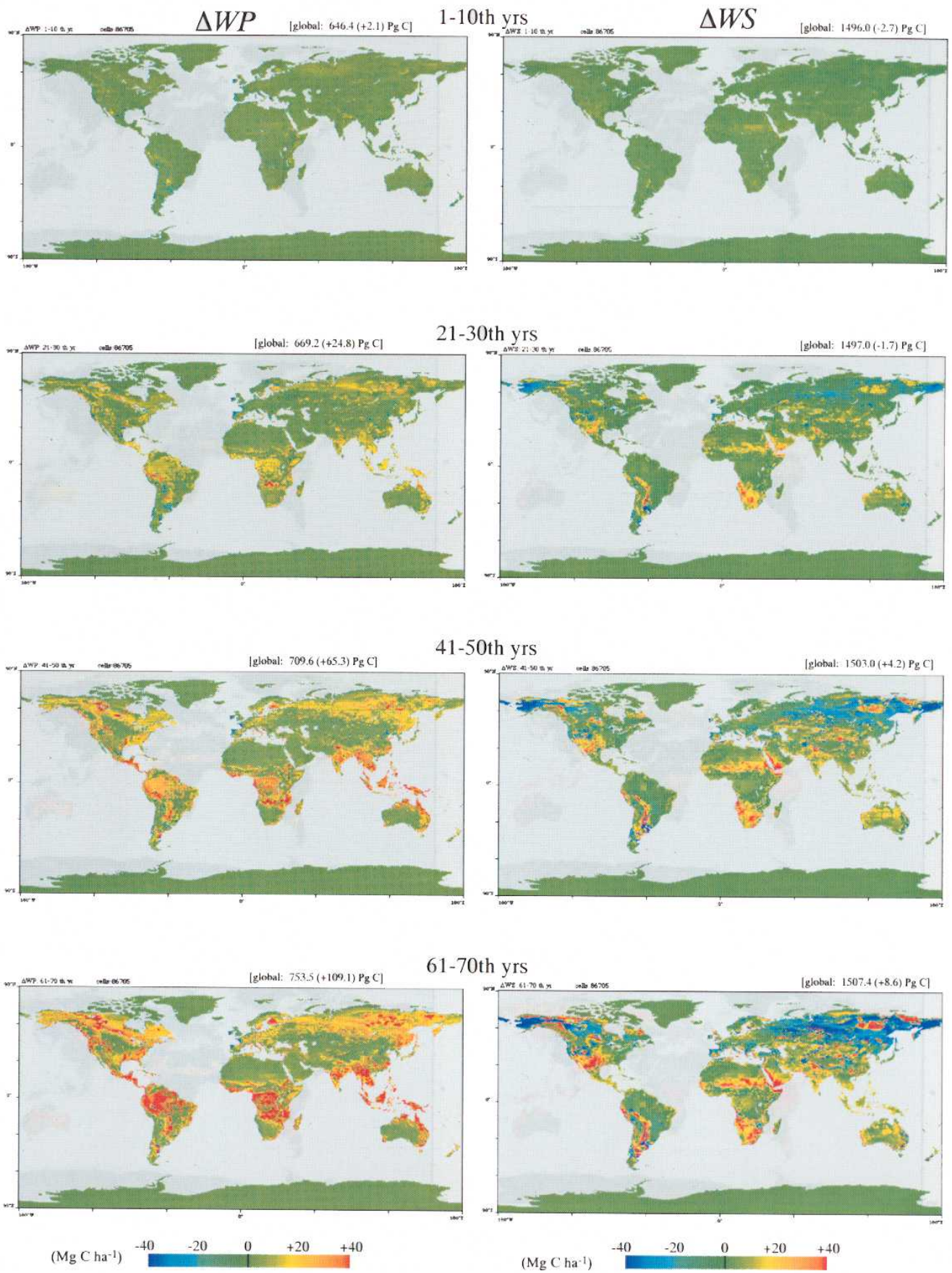

Fig. 6-8 (continued). Estimated changes in (left) plant carbon storage *WP* and (wight) soil carbon storage *WS*, under GISS climate projection with gradual CO_2 doubling.

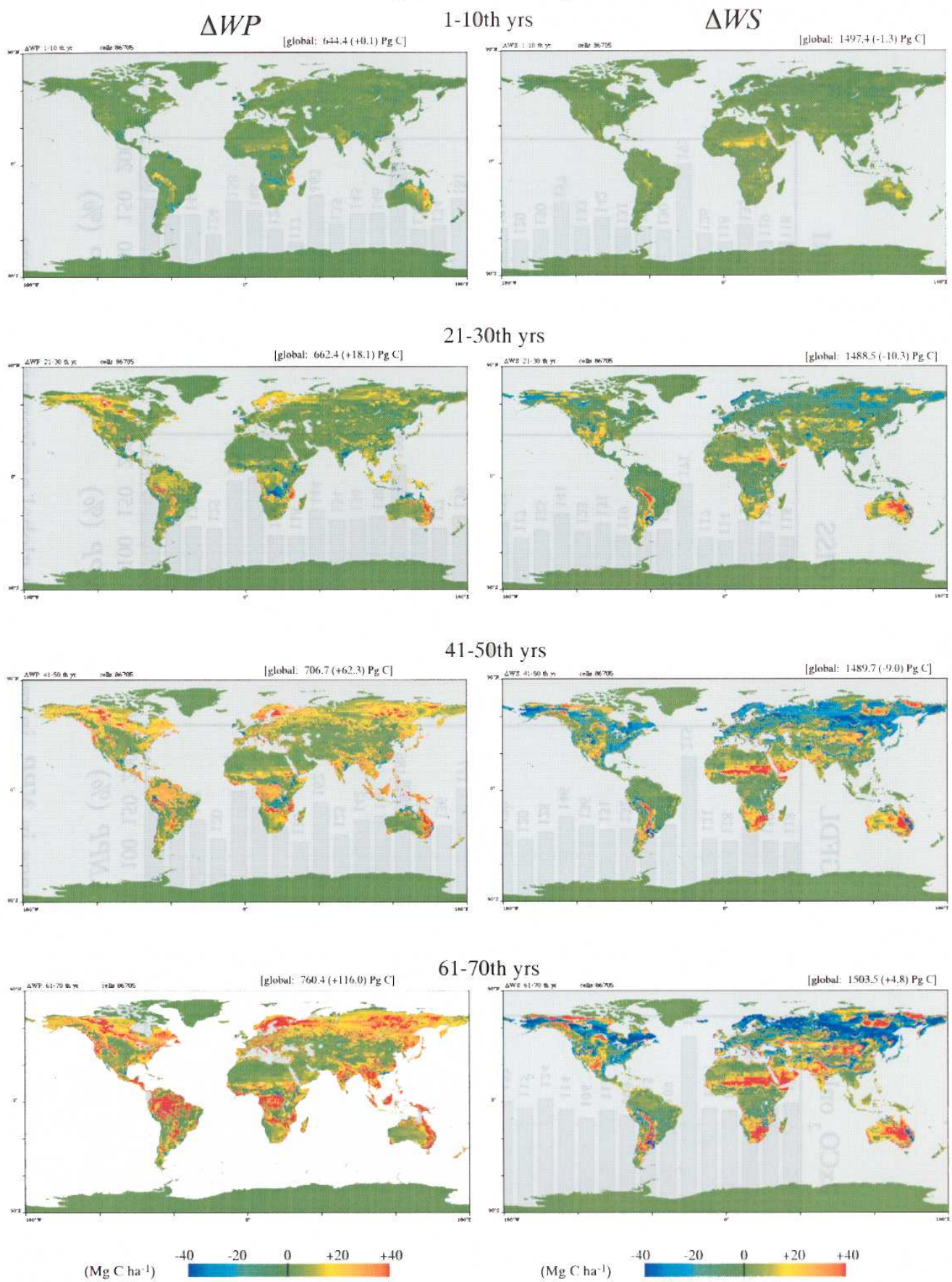

Fig. 6-8 (continued). Estimated changes in (left) plant carbon storage *WP* and (right) soil carbon storage *WS*, under MRI climate projection with gradual CO_2 doubling.

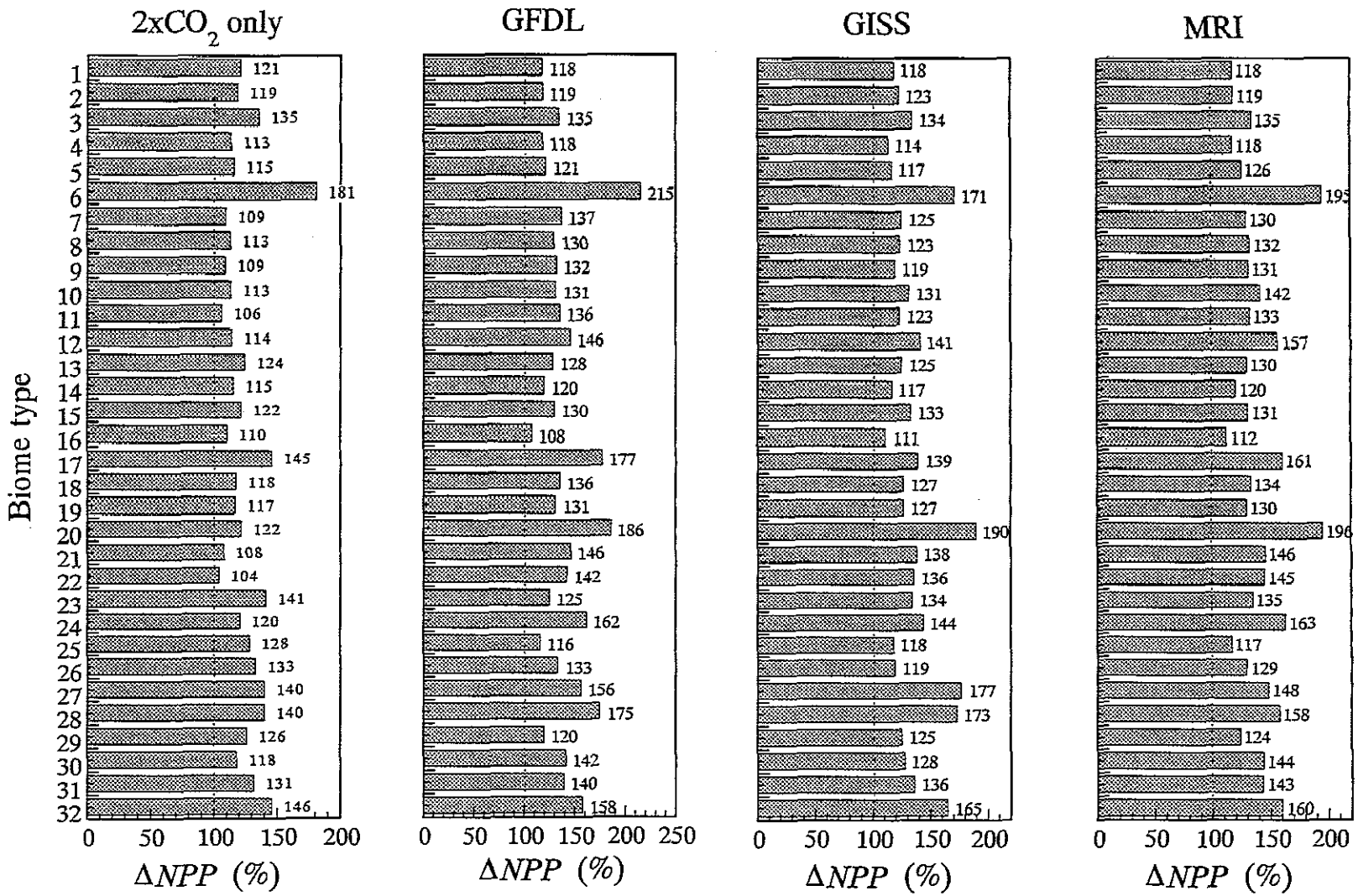

Fig. 6-9. Biome-specific change in *NPP*, in response to global environmental change, estimated by Sim-CYCLE prediction run (average of 66th to 70th years)

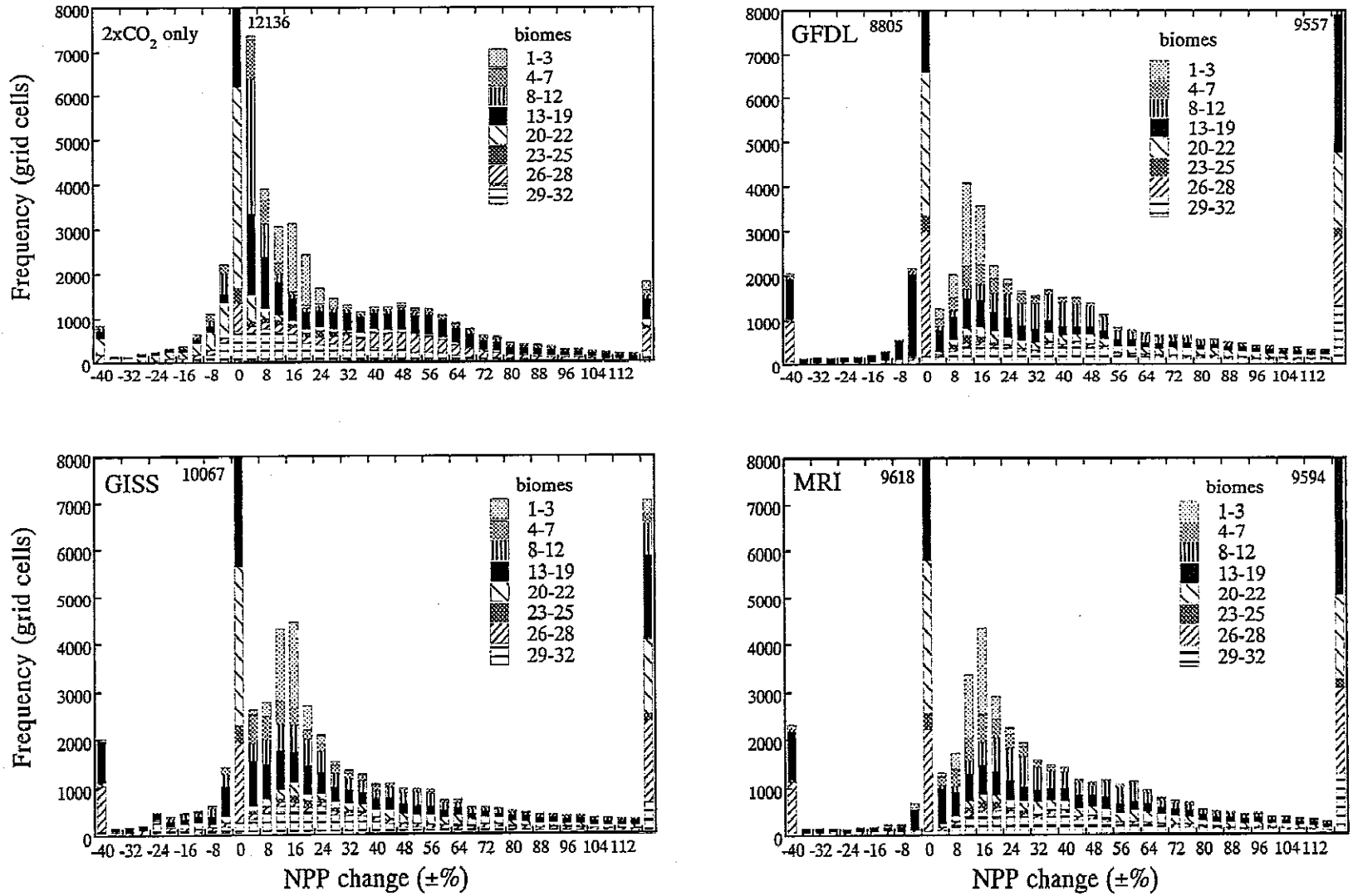

Fig. 6-10. Frequency distribution of *NPP* change as a consequence of global environmental change, estimated by Sim-CYCLE prediction run, at the 70th year.

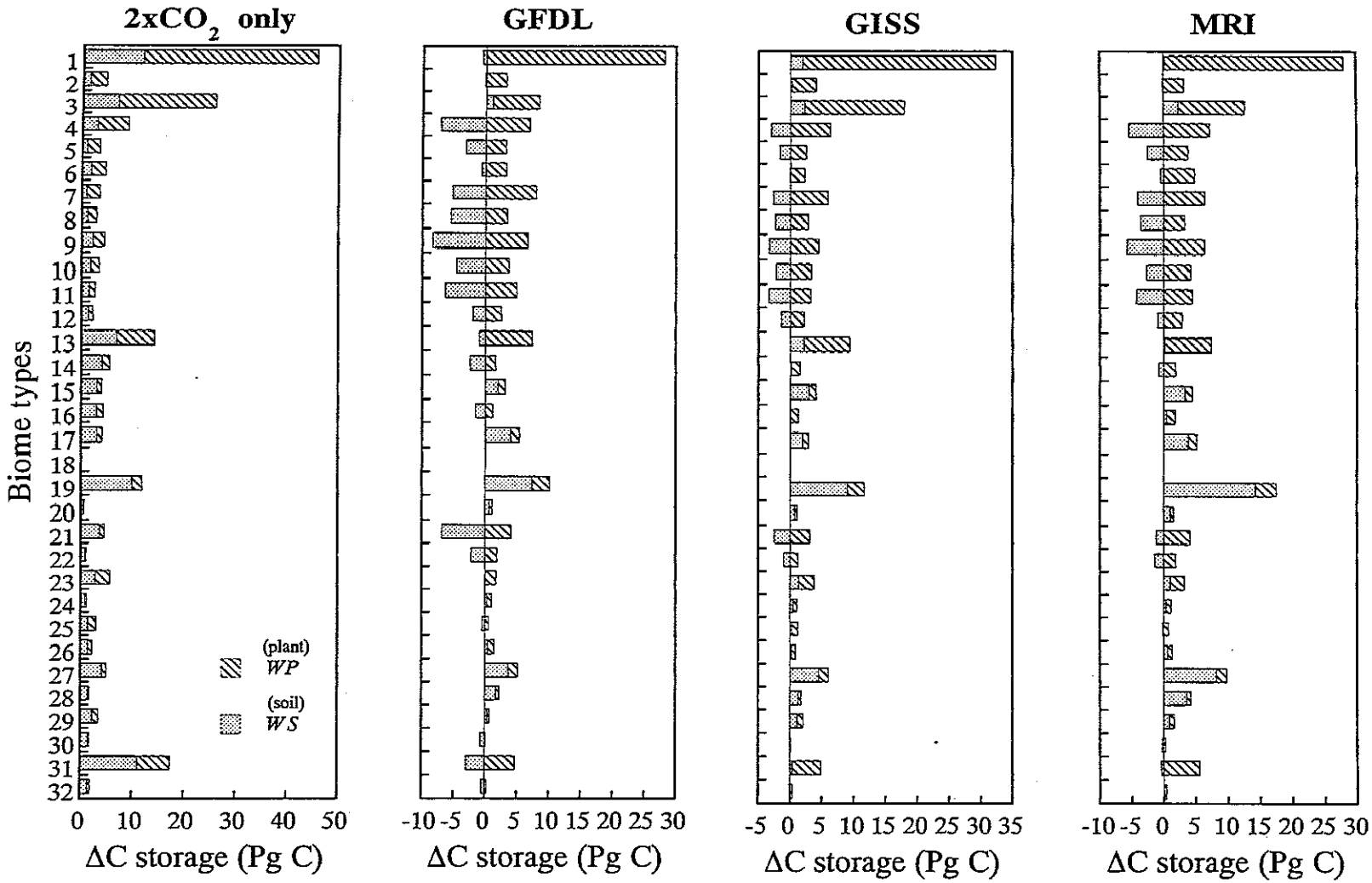

Fig. 6-11. Biome-specific change in carbon storage, in response to global environmental change, estimated by Sim-CYCLE prediction run (average of 66th to 70th years)

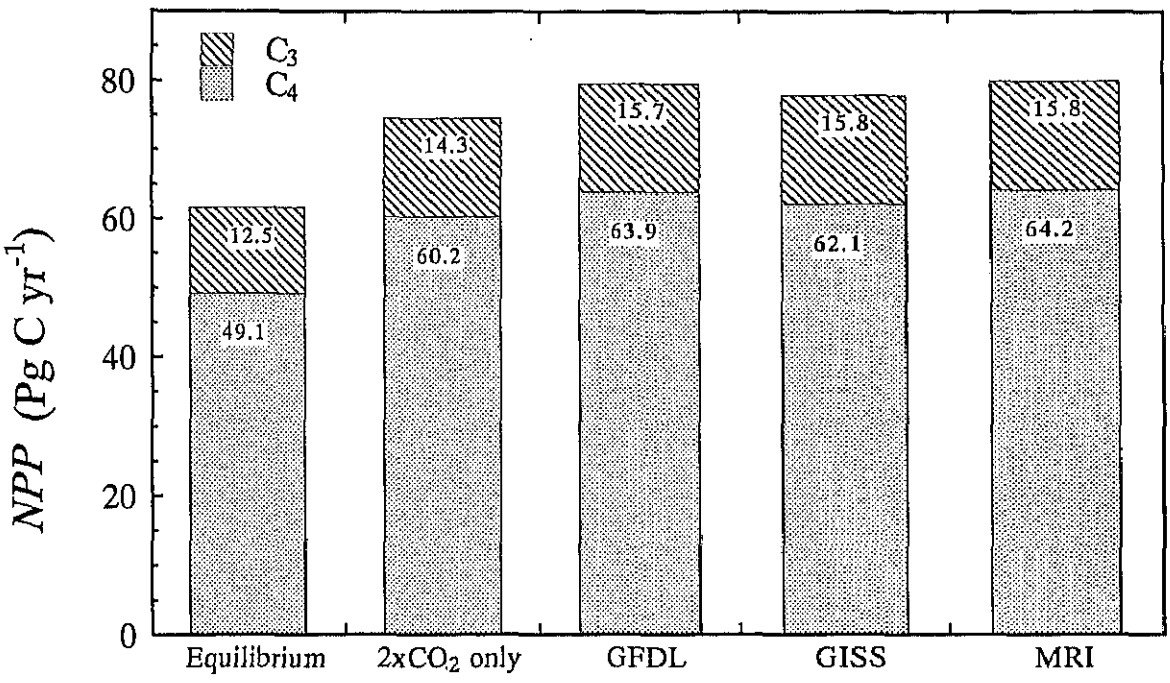

Fig. 6-12. Estimated change in *NPP* of C_3 and C_4 plants, for each global change scenario.

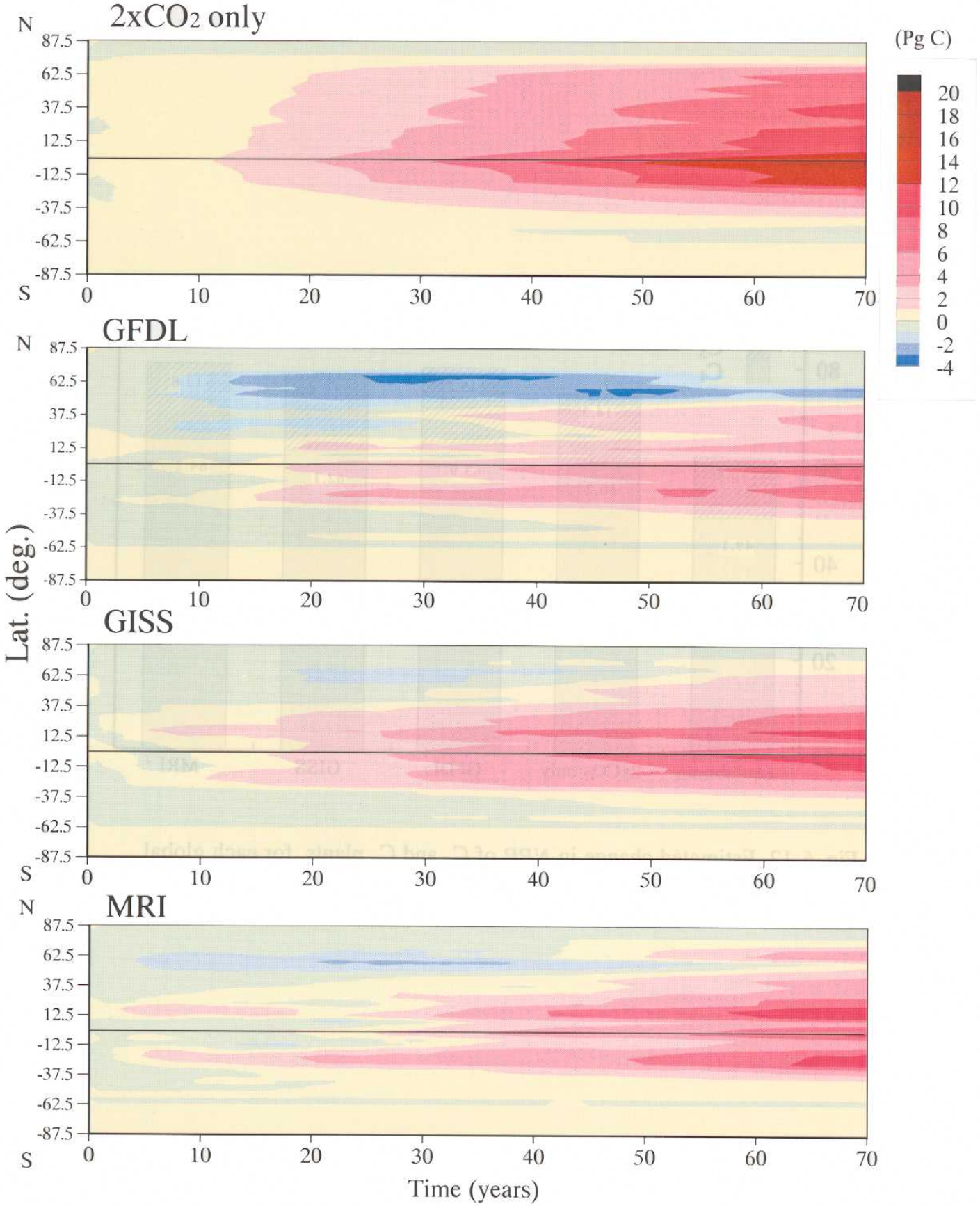

Fig. 6-13. Latitudinal distribution of cumulative change in the ecosystem carbon storage along 5°-resolution latitudinal bands over the period of 70 years.

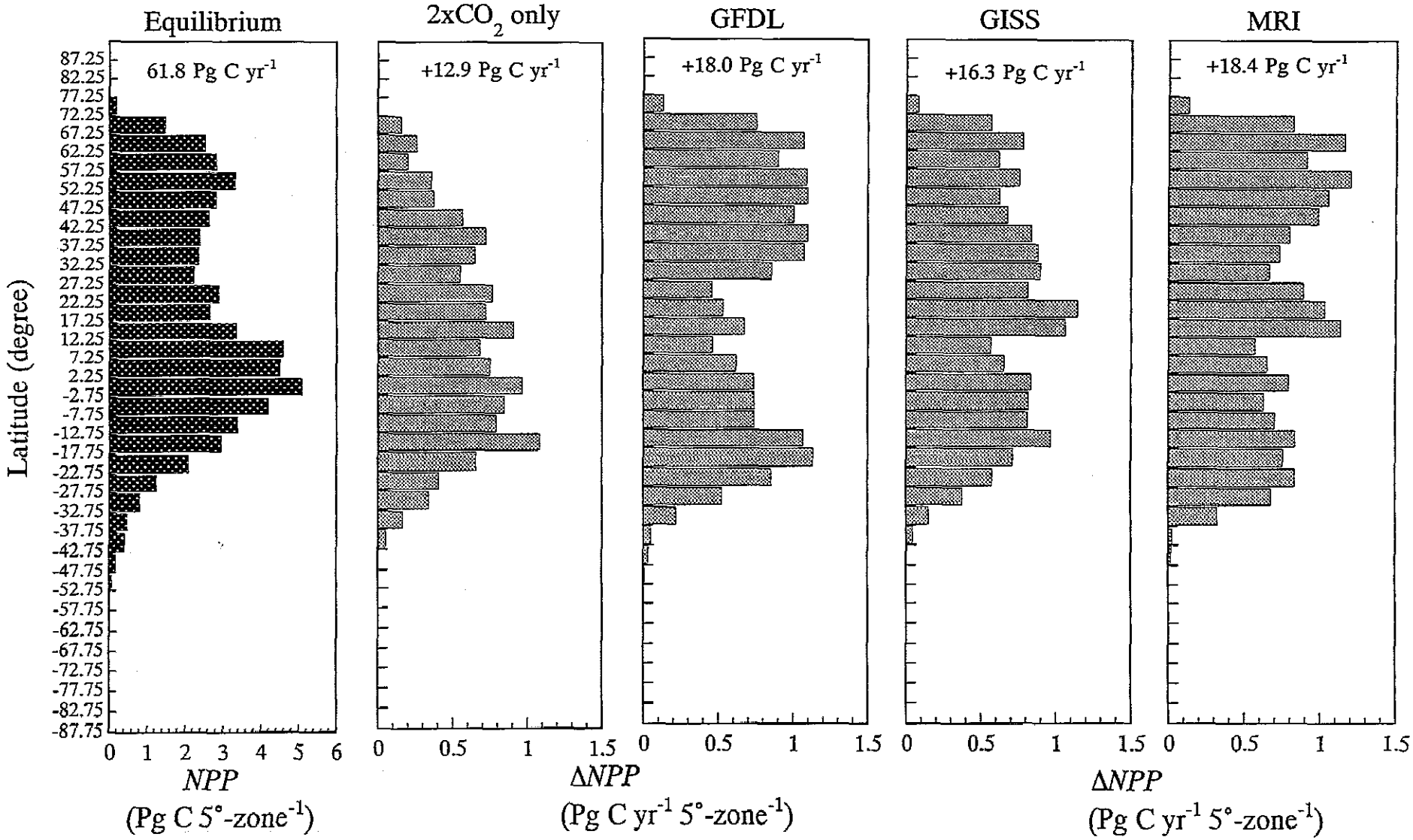

Fig. 6-14. Latitudinal distribution of *NPP* change. (a) Control state, and Δ*NPP* of (b) CO_2 change only, (b) GFDL climate, (c) GISS climate, and (d) MRI climate

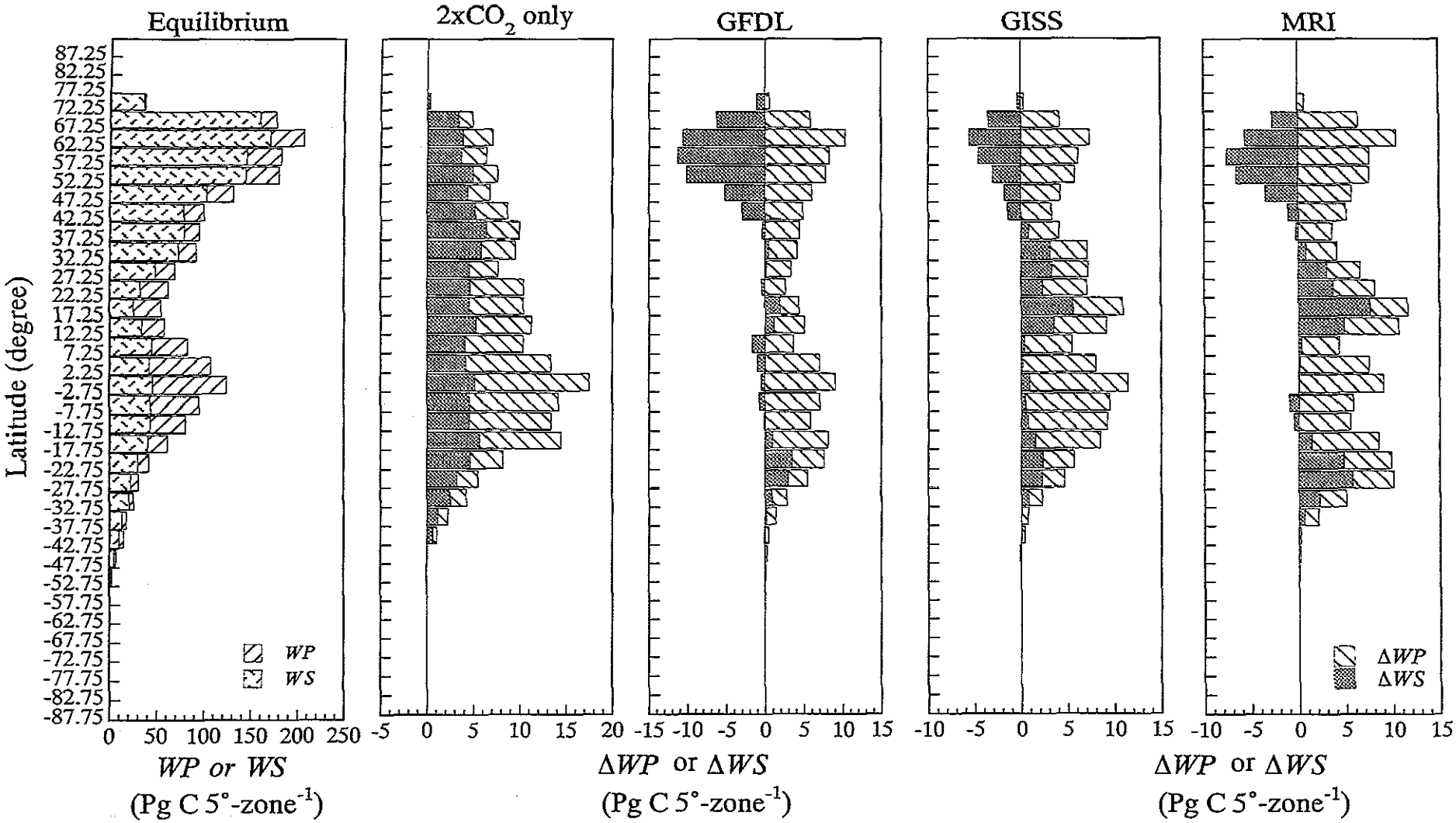

Fig. 6-15. Latitudinal distribution of carbon storage change. (a) Control state, and ΔWP and ΔWS of (b) CO_2 change only, (b) GFDL climate, (c) GISS climate, and (d) MRI climate

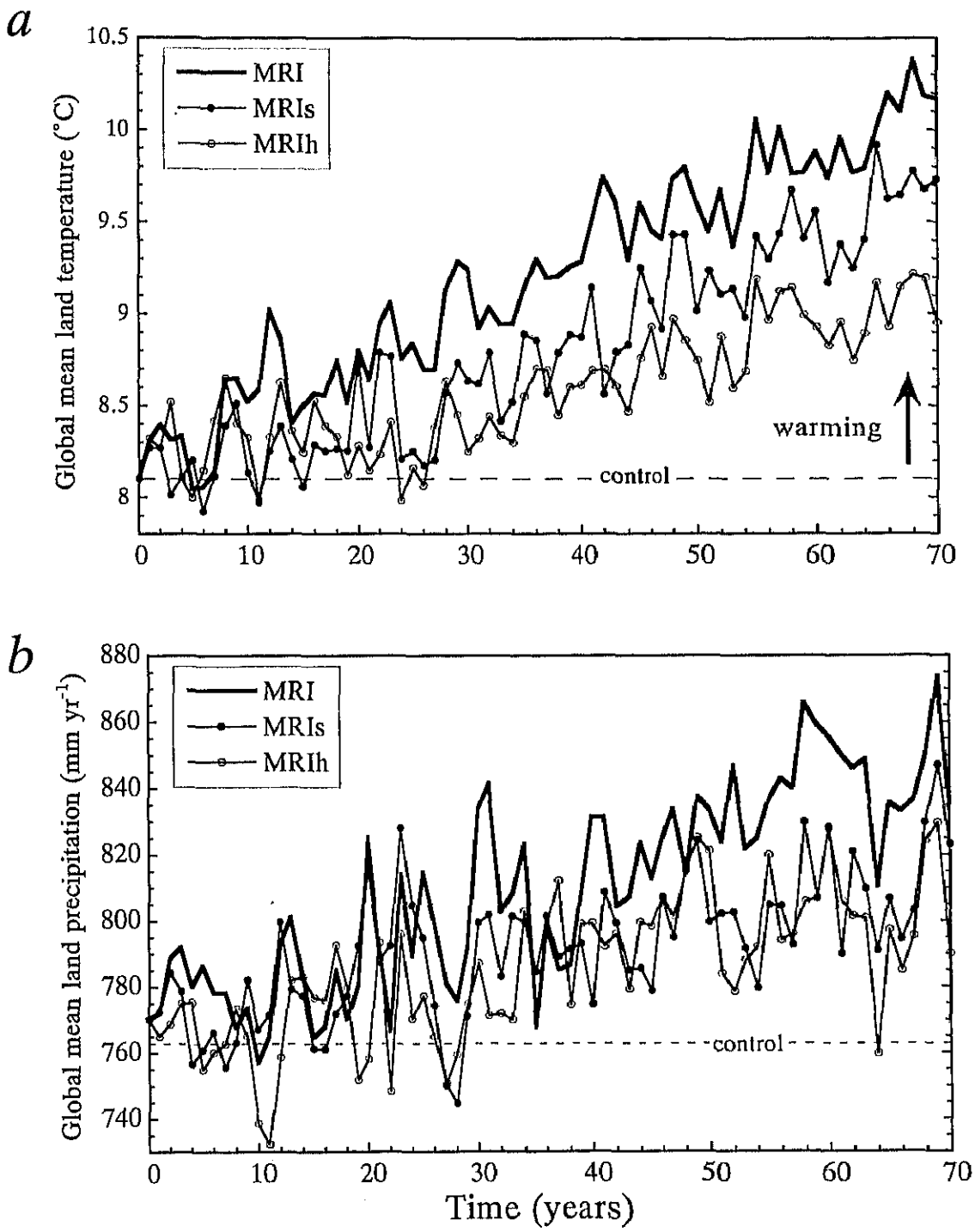

Fig. 6-16. Climate projection by three scenarios (MRI, MRIs, and MRIh). (a) Global mean land temperature and (b) global mean land precipitation.

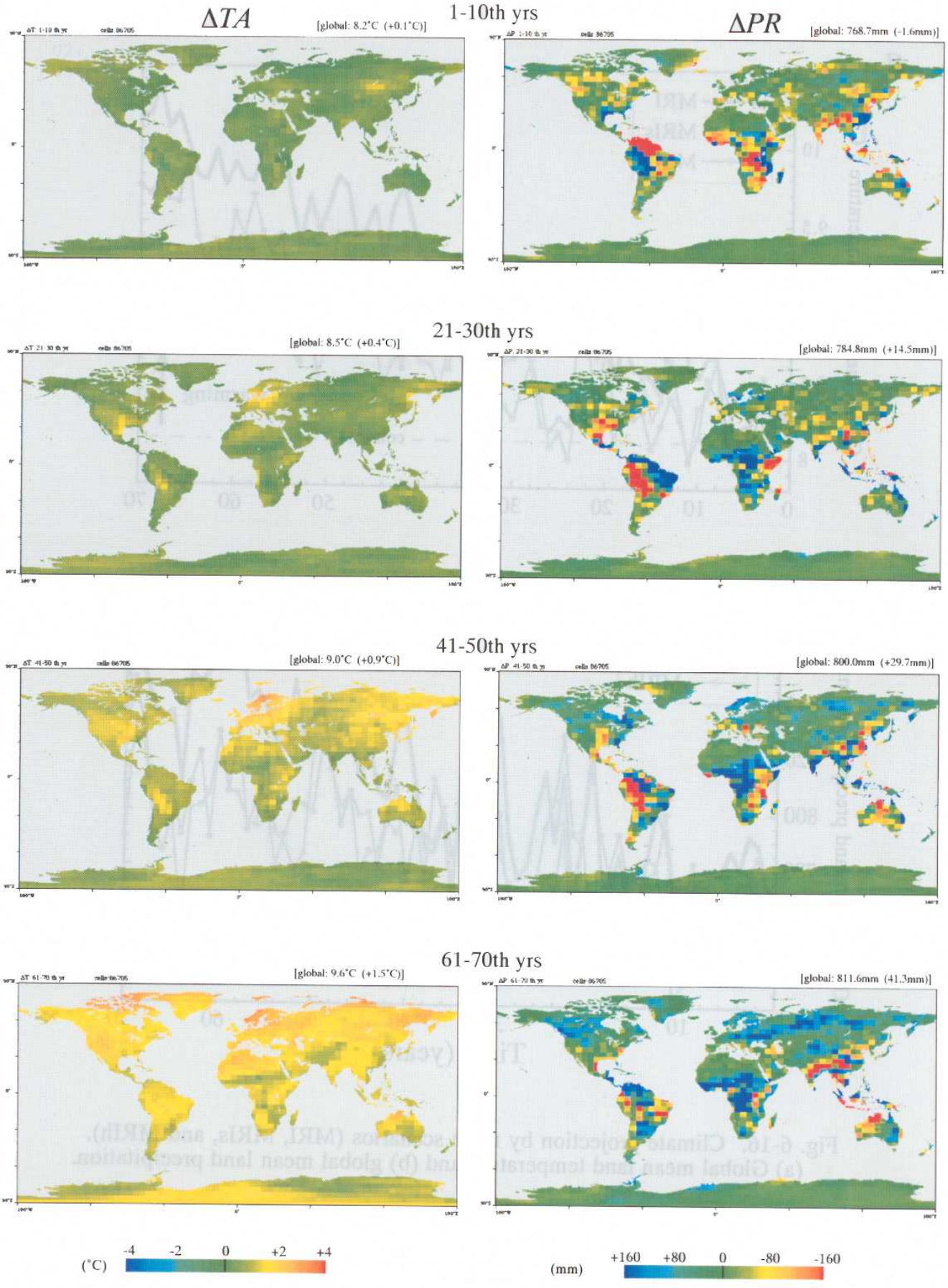

Fig. 6-17. Projected climate change scenarion by MRIs gradual CO_2 doubling simulation.

(MRIh scenario)

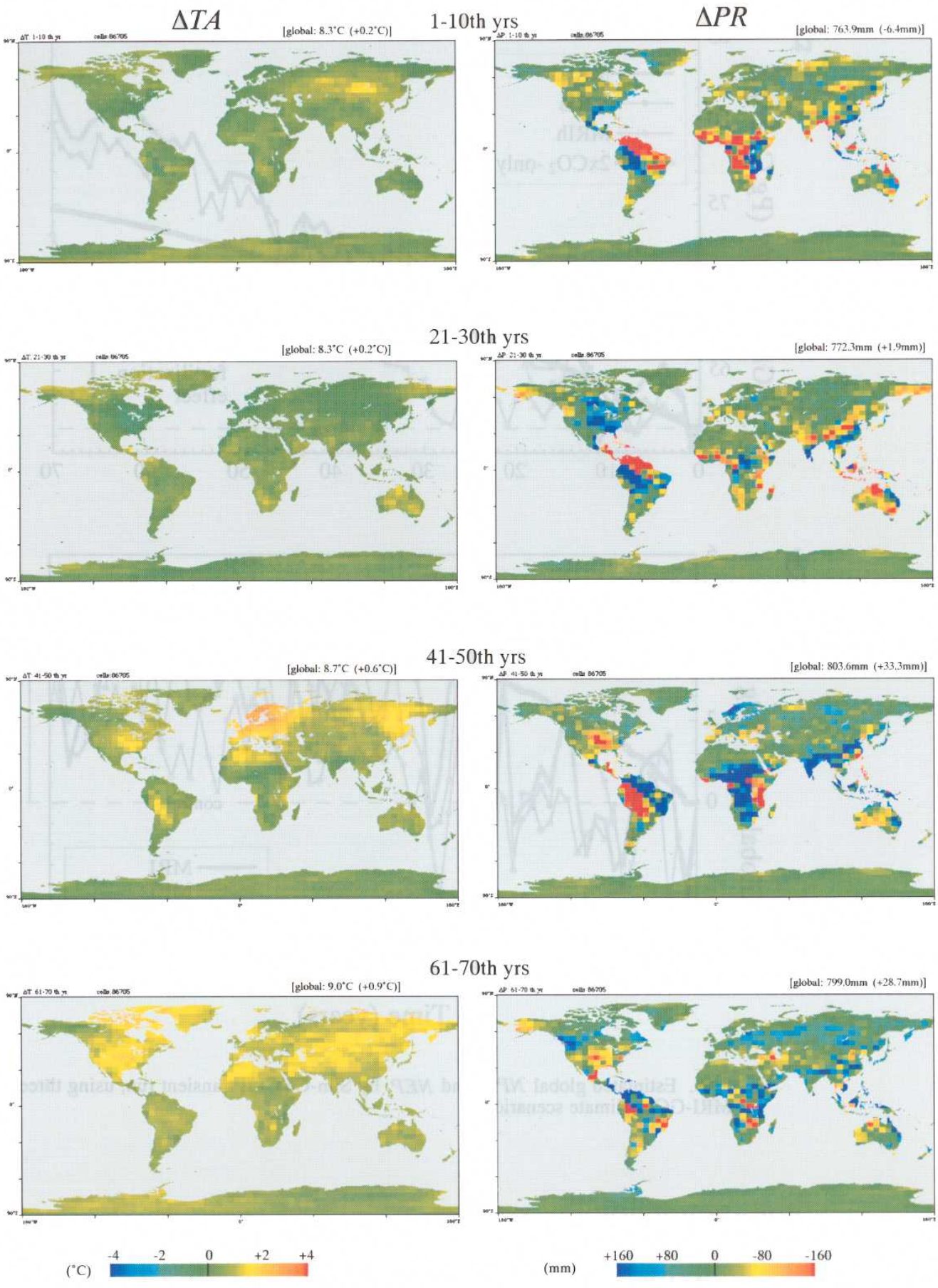

Fig. 6-17 (continued). Projected climate change scenarion by MRIh gradual CO_2 doubling simulation.

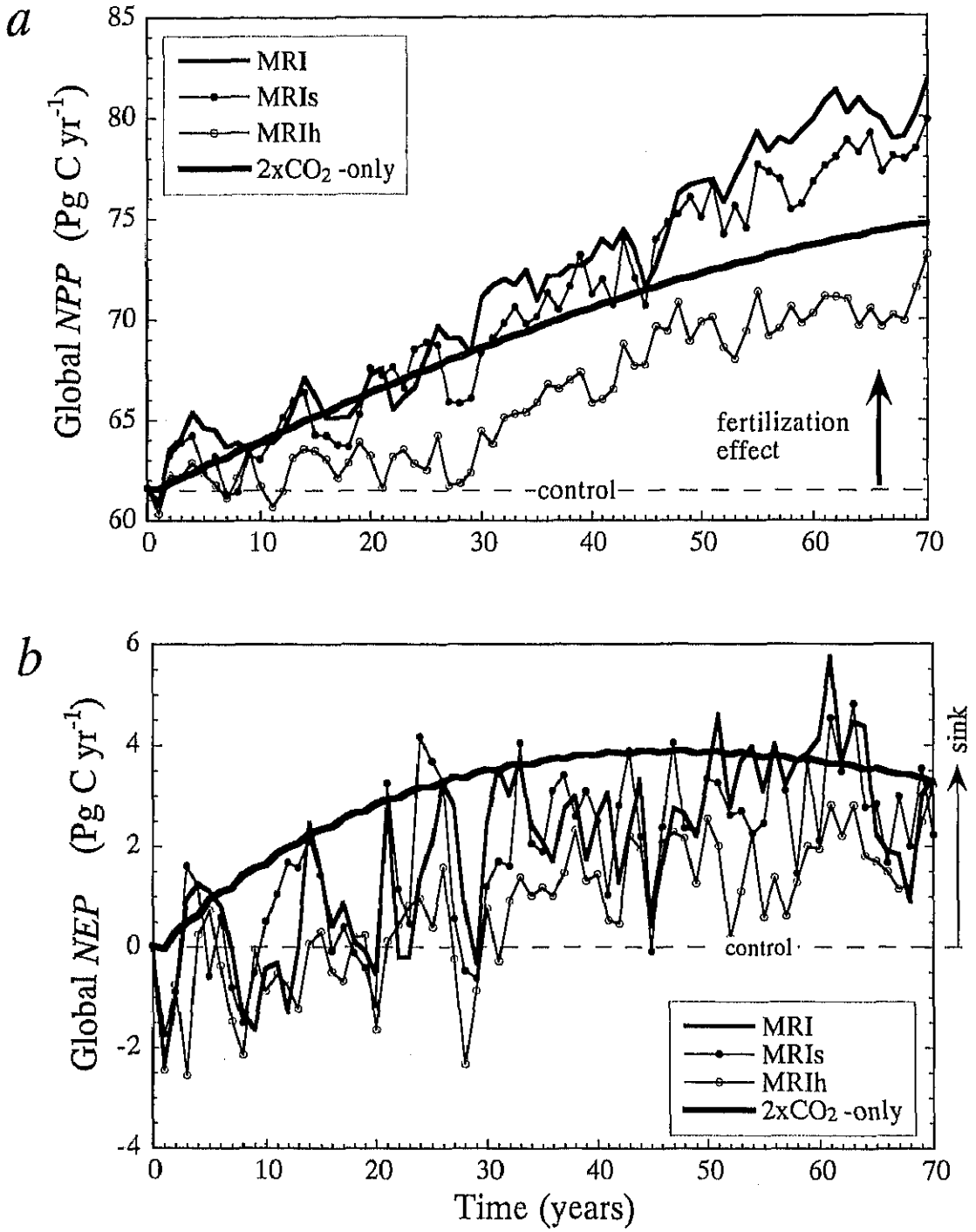

Fig. 6-18. Estimated global *NPP* and *NEP* by Sim-CYCLE transient run, using three MRI-GCM climate scenarios.

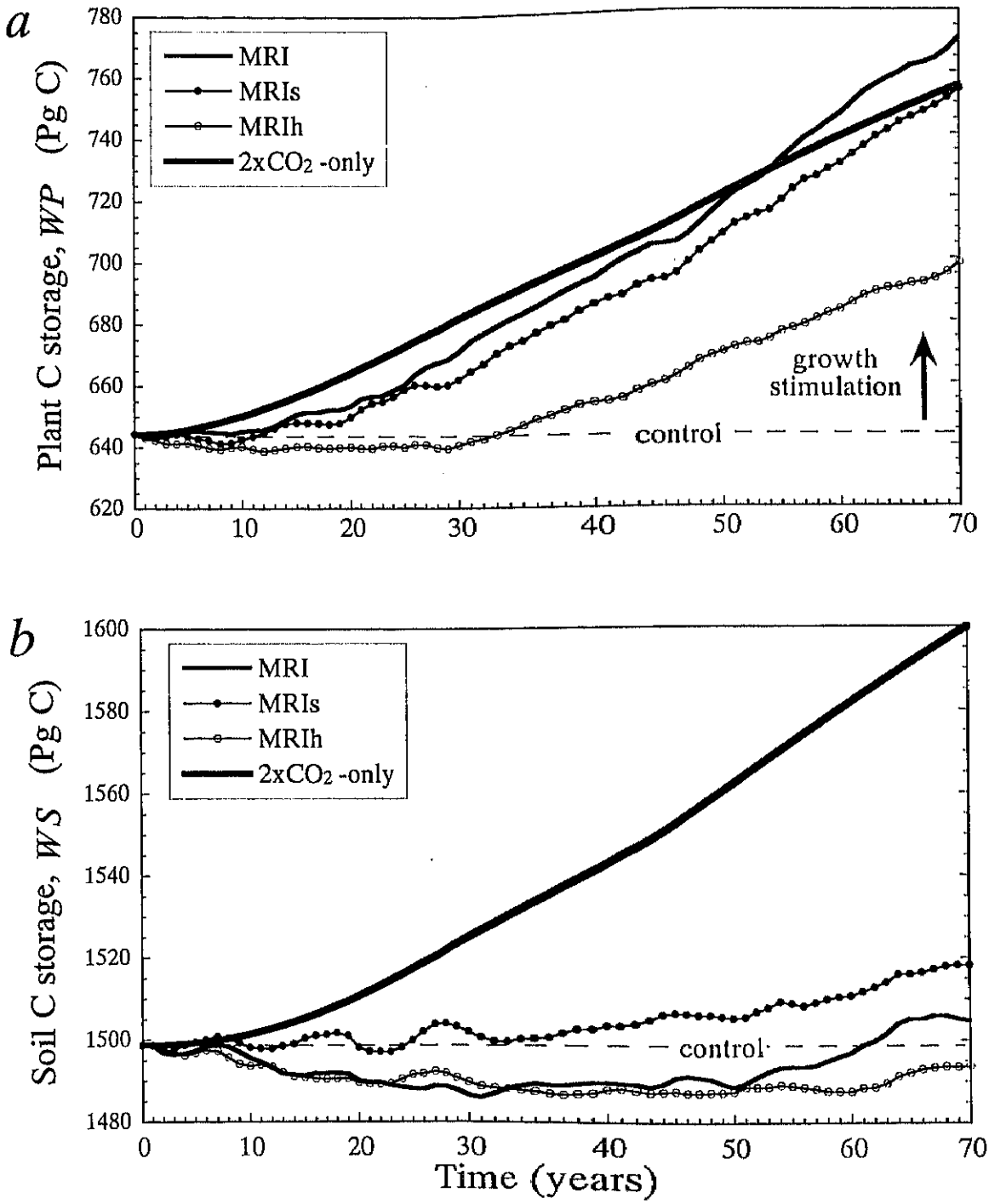

Fig. 6-19. Estimated change in (a) plant carbon storage WP and (b) soil carbon storage WS .

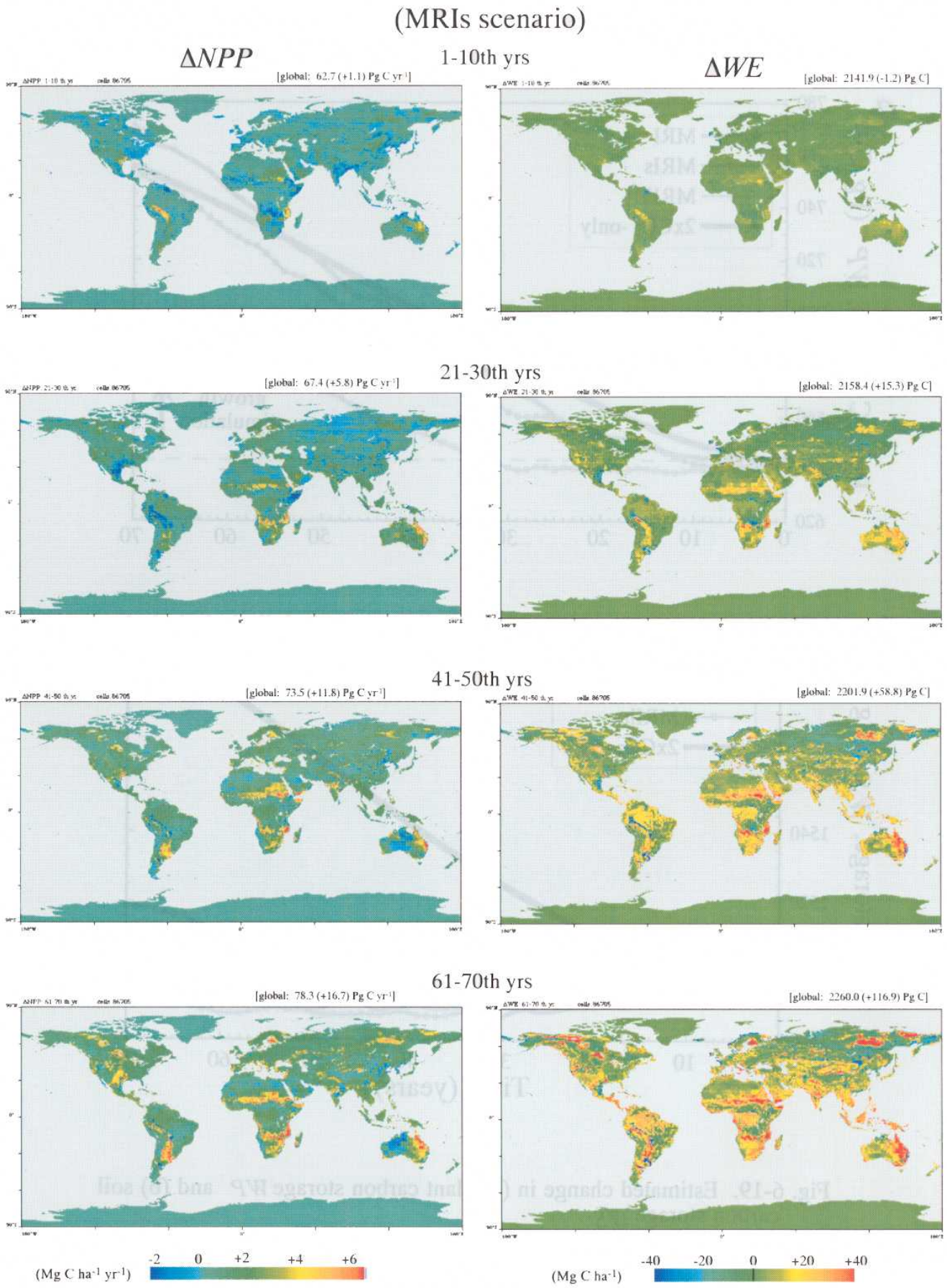

Fig. 6-20. Estimated changes in (left) *NPP* and (right) carbon storage *WE*, under MRIs climate projection with gradual CO_2 doubling.

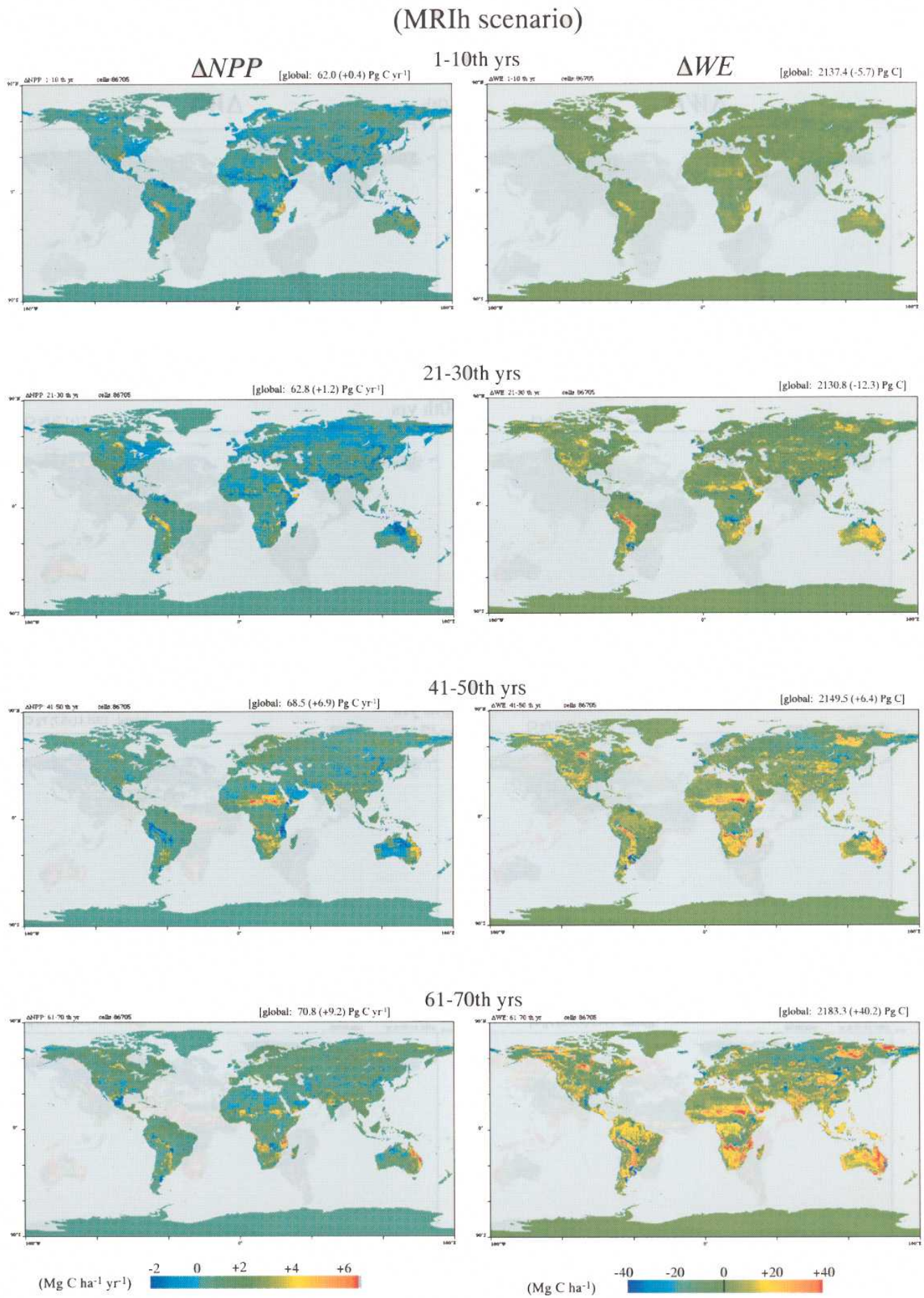

Fig. 6-20 (continued). Estimated changes in (left) *NPP* and (right) carbon storage *WE*, under MRIh climate projection with gradual CO_2 doubling.

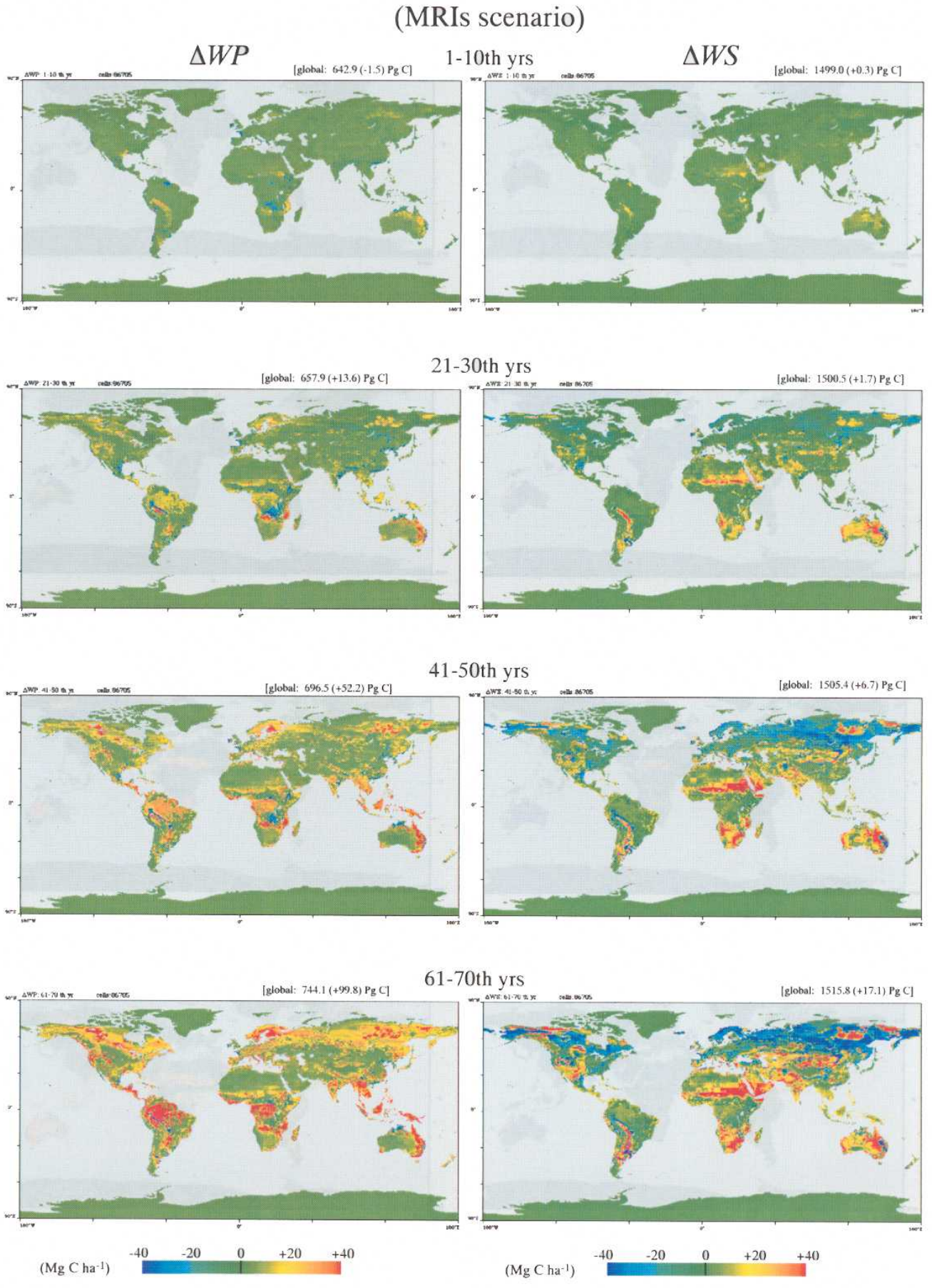

Fig. 6-21. Estimated changes in (left) plant carbon storage *WP* and (right) soil carbon storage *WS*, under MRIs climate projection with gradual CO_2 doubling.

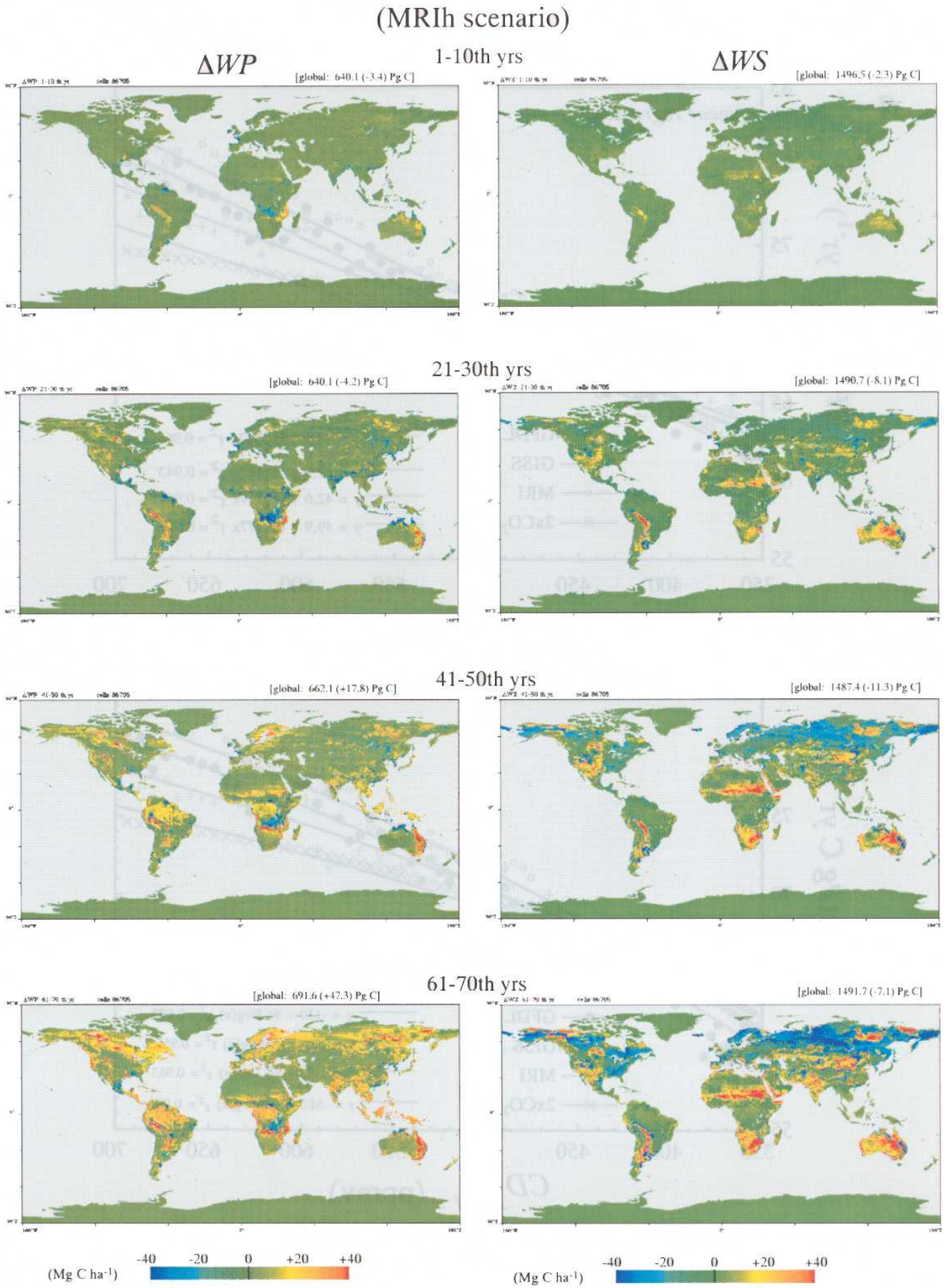

Fig. 6-21 (continued). Estimated changes in (left) plant carbon storage *WP* and (right) soil carbon storage *WS*, under MRIh climate projection with gradual CO_2 doubling.

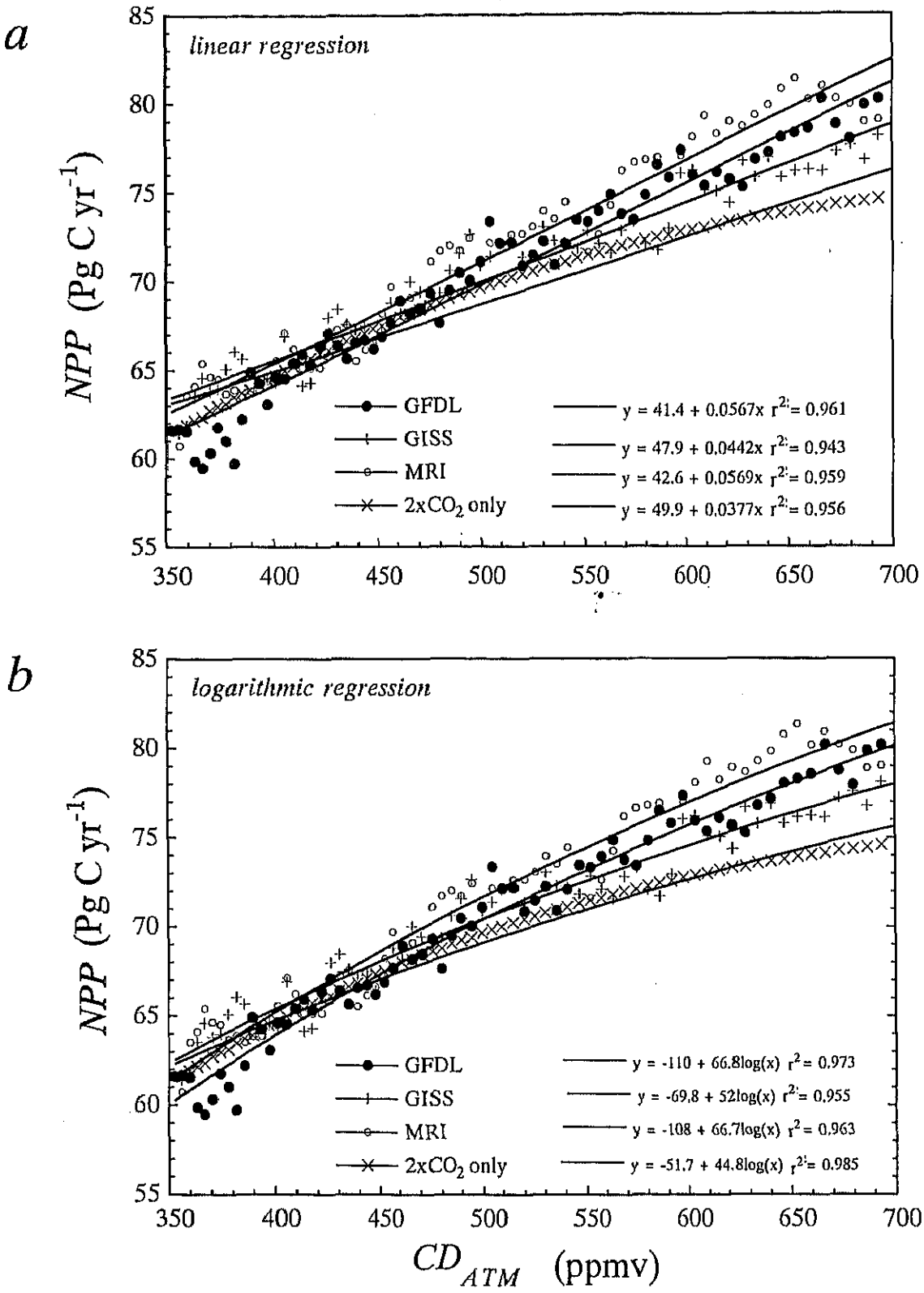

Fig. 6-22. Relationship between atmospheric CO_2 concentration (CD_{ATM}) and total *NPP*, estimated by Sim-CYCLE prediction run using GCM scenarios. (a) Linear regression, and (b) logarithmic regression.

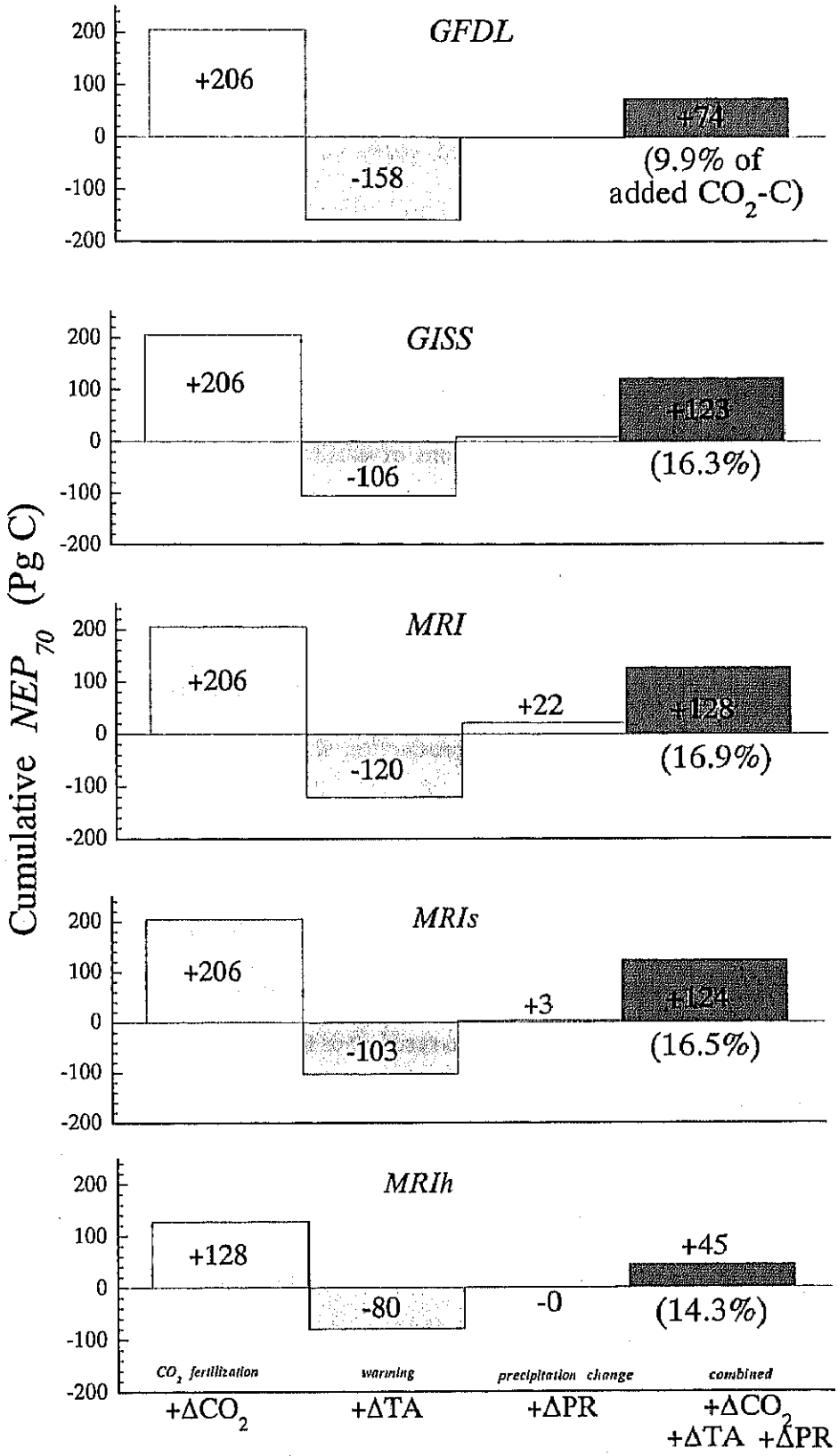

Fig. 6-23. Impacts of global change on net biospheric carbon balance, estimated by Sim-CYCLE 70-year run using three GCM scenarios. Values are shown for individual and multiplicative changes.